POLITECNICO DI TORINO

Master's Degree in Aerospace Engineering

Academic Year 2022-2023

Reentry corridor reference trajectory definition

Supervisors

Prof. Lorenzo CASALINO

Ing. Martins SUDARS

Ing. Giorgio FASANO

Candidate

Simone CASTELLO

Table of Contents

List of Figures

Acronyms

GNC
> Guidance Navigation and Control

EIP
> Entry Interface Point

LEO
> Low Earth Orbit

FPA
> Flight Path Angle

L/D
> Lift to Drag ratio

IXV
> Intermediate eXperimental Vehicle

ECEF
> Earth Centered Earth Fixed

GPS
> Global Positioning System

DRS
> Descent and Recovery System

3-DoF
> Three Degrees of Freedom

AoA

Angle of Attack

PD

Proportional Derivative

PID

Proportional Integrative Derivative

D-V

Drag-Velocity

RAAN

Right Ascension of the Ascending Node

TAEM

Terminal Area Energy Management

NLP

Non Linear Programming

BVP

Boundary Value Programming

PMP

Pontryagin Maximum Principle

BBO

Black Box Optimization

SQP

Sequential Quadratic Programming

Chapter 1

Introduction

Figure 1.1: Illustration of Orion capsule re-entry

Atmospheric re-entry is an important aspect of many space missions: it is crucial for every human mission to guarantee a safe landing of the crew and it is also necessary whenever experiments or samples need to be transported back to Earth. This problem has also implications in the military field, just think about Inter Continental Ballistic Missiles (ICBMs) or the more advanced hypersonic missiles being developed today.

The first re-entry vehicle was developed in 1952 by General Electric and it was called the Mark 2, designed for Thor, Jupiter and Atlas missiles [1]. It was a ballistic capsule with a blunt body shape and a heat sink designed to absorb

the heat from re-entry. Since then many other vehicles were designed and the technological level improved rapidly: there were advancements in the heat shield design with the introduction of the ablative technology that allowed for higher total heat loads and significantly lower masses, and the radiative technology that could be reused such in the case of Space Shuttle. There were improvements also from an aerodynamic point of view with the development of lifting body re-entry vehicles: they have great control authority and can be guided with high accuracy, they are also subject to much lower G-loads and thus ideal for human flight.

This thesis focuses on lifting body re-entry vehicles on Earth atmosphere and has three main goals:

- Developing a tool that allows the derivation of lifted re-entry trajectories satisfying every mission constraint. To achieve this goal an optimization approach must be utilized.

- Development and implementation of a guidance and control algorithm for 3 degrees of freedom flight simulation, able to follow the optimal reference trajectory profile.

- Test the model and compare the results with existing re-entry vehicles.

The chapters 2, 4, 5 and 6 will discuss in depth the characteristics of the re-entry problem and how it has been approached. There will be a detailed discussion about the developed model form the trajectory optimization aspect to the guidance and control aspect. In chapter 7 the results will be shown to prove the efficacy and robustness of the algorithms.

Chapter 2

Overall problem statement

In this chapter the overall re-entry problem is described in every aspect [2]. Every section covers a different aspect:

- **The re-entry problem**
  Here an overview on re-entry with the various strategies relative to the different vehicles is described.

- **Constraints**
  The numerous constraints are listed here: there are physical constraints relative to the vehicle characteristics and structural/thermodynamic limits, geographical constraints such as the avoidance of certain no-fly zones and ground station visibility constraints.

- **Target**
  This section describes the desired target values at the end of the trajectory, they are necessary to connect the re-entry part to the Terminal Area Energy Management (TAEM) part. The TAEM is the last part of the trajectory where the vehicle is controlled in order to land to the desired spot, the GNC strategy completely changes in this part which is not covered in this thesis.

- **Entry corridor**
  A crucial aspect of the re-entry problem is the definition of the entry corridor which defines a region of survivability of the vehicle. It is described in this section.

- **Vehicle dynamics**
  The vehicle dynamics equations and the overall mathematical model used in this thesis is described here.

- **IXV entry vehicle**
  In this section a brief description of the IXV vehicle is depicted, this spacecraft is the main reference for the validation of the results obtained in this thesis.

This chapter describes the background knowledge necessary to understand the rest of the thesis.

2.1 The re-entry problem

The main goal of atmospheric re-entry is to safely guide and land the entry vehicle. During descent the spacecraft is subject to significant structural and thermodynamic stresses that must not exceed the design limits. The Guidance Navigation and Control (GNC) subsystem of the vehicle has to precisely follow a predetermined reference trajectory that satisfies the numerous constraints in order to survive and meet every required target condition [3].

The re-entry starts at the Entry Interface Point (EIP), that is where the aerodynamic forces are no longer negligible at a height of around 120 *km*. The EIP velocity ranges from about 7500 *m/s* for an equatorial prograde orbit to about 8500 *m/s* for an equatorial retrograde orbit considering re-entry from LEO (400 to 800 *km* height). Another important EIP parameter is the Flight Path Angle (FPA), which defines the steepness of the entry condition. If the FPA is too small the spacecraft rebounds on the atmosphere and skips back to space; instead, if it is too steep, the vehicle enters the atmosphere with an excessive descent rate and reaches the denser parts too early with high heat fluxes and G-loads.

There are three possible re-entry scenarios:

- **Ballistic re-entry**
  It occurs when the Lift-to-Drag ratio (L/D) is 0, this is the case of meteoroids or the Mercury capsule. The control authority is zero and the trajectory is fully determined by the EIP conditions and the ballistic coefficient of the vehicle. This trajectory is characterized by an elevated heat flux and G-load.

- **Aerodynamic re-entry**
  In this case L/D > 0, the vehicle is able to control the trajectory by moving the lift vector (typically with a bank manoeuvre). This way it is possible to obtain a much lower heat flux and G-load which is convenient for human re-entry and for some kinds of payloads. An example is the Space Shuttle or the European IXV vehicle. A controlled re-entry also means higher accuracy on the landing position.

- **Skip re-entry**
  The vehicle enters the atmosphere with a combination of FPA and Angle of Attack (AoA) such that it rebounds on it. After some time the spacecraft reenters the atmosphere with a lower entry velocity. It is the case of the Orion capsule for Artemis missions.
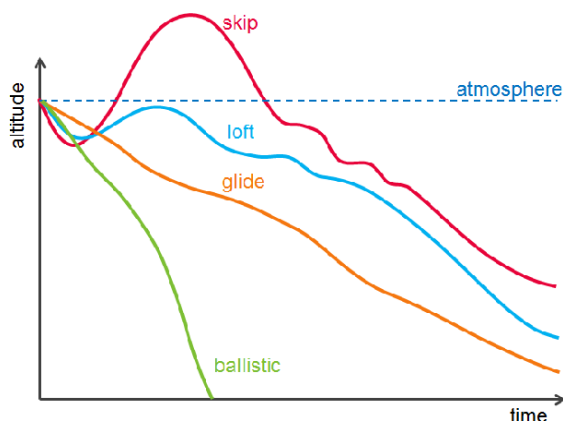
Figure 2.1: Comparison between the different re-entry strategies

2.2 Constraints

The entry vehicle must satisfy a wide range of constraints such as thermodynamic and structural limits, geographical constraints, visibility constraints and so on. The following section describes every constraint considered in this study along with the relative equations:

- **Maximum dynamic pressure**
  The re-entry vehicle is designed to withstand a maximum value of dynamic pressure. The general expression of dynamic pressure is the following:

$$q = \frac{1}{2}\rho v^2 < q_{max} \tag{2.1}$$

ρ: atmospheric density
v: spacecraft velocity
q: dynamic pressure
q_{max}: maximum allowed dynamic pressure

5

Another constraint is the pressure on the stagnation point, which has the following expression:

$$q_{stag} = 1{,}85q < q_{stag_{max}} \tag{2.2}$$

q_{stag}: pressure at the stagnation point
q: dynamic pressure
$q_{stag_{max}}$: maximum allowed pressure at the stagnation point

- **Maximum load factor**
  Due to structural reasons a maximum value of load factor (G-load) can be tolerated by the spacecraft. The G-load value can be easily calculated with the following expression:

$$g_{load} = \frac{\sqrt{L^2 + D^2}}{mg_0} < g_{load_{max}} \tag{2.3}$$

L: spacecraft lift
D: spacecraft drag
m: spacecraft mass
g_0: gravitational acceleration at sea level
g_{load}: load factor
$g_{load_{max}}$: maximum allowed load factor

- **Maximum heat flux**
  Any kind of heat shield can withstand a maximum value of heat flux per unit area, this limit is generally higher in ablative heat shields compared to radiative heat shields (the latter is the technology used in the vehicles analysed in this thesis). There are many ways to calculate this heat flux, an approximated empiric equation used to achieve this goal is the DKR formula:

$$\tilde{q} = K catal \frac{1}{\sqrt{R_n}} \left(\frac{\rho}{\rho_0}\right)^{0,5} \left(\frac{v}{v_0}\right)^{3,15} < \tilde{q}_{max} \tag{2.4}$$

$catal$: catalytic coefficient
R_n: spacecraft nose radius
ρ: atmospheric density
v: spacecraft velocity
$\tilde{q}$: nose heat flux

6

$\tilde{q}_{max}$: maximum allowed nose heat flux
$K = 113{,}5 \cdot 10^6$
$\rho_0 = 1.225 \; kg/m^3$
$v_0 = 7908 \; m/s$

This formula evaluates only the conductive heat flux, the radiative term can be neglected since it becomes significant at velocities above 9 km/s which are higher than the entry velocities considered in this thesis. For the specific cases of IXV and Space Rider entry vehicles a more accurate aero-thermodynamic database is used to calculate the heat fluxes.

- **Maximum flap heat flux**
  The flaps are generally subject to a higher heat flux compared to the rest of the vehicle. There is not an analytical expression for the evaluation of this heat flux: it can only be interpolated from the aero-thermodynamic database relative to the given spacecraft. In the case of this study the IXV database has been used.

- **Maximum integral heat flux**
  The vehicle can sustain a maximum heat load:

$$\tilde{Q} = \int_0^T \tilde{q} \, dt < \tilde{Q}_{max} \tag{2.5}$$

$\tilde{Q}$: total heat load
$\tilde{q}$: heat flux
$\tilde{Q}_{max}$: maximum allowed heat load

- **Ceiling limit**
  The ceiling limit represents the maximum height at which equilibrium glide can be sustained. The vehicle can fly above this limit just in a transitory state, but it is not recommended because the dynamic pressure decreases significantly and thus the control authority of the spacecraft degrades. The ceiling is not a destructive constraint but it is important to fly below this limit to maintain full control of the vehicle. To calculate the ceiling firstly the bank angle and the flight path angle are set to zero and then the generated lift is put equal to the gravitational force acting on the vehicle minus the centrifugal force. In ECEF coordinates the following expression is derived:

$$\frac{1}{2}\rho v^2 S C_l = m\left(\left(g - \frac{v^2}{r}\right) - 2\Omega v \cos\phi \sin\psi - \Omega^2 r \cos\phi^2\right) \tag{2.6}$$

S: spacecraft reference surface
C_l: spacecraft lift coefficient
ρ: atmospheric density
v: spacecraft velocity
r: distance from the center of the Earth
g: gravitational acceleration
Ω: Earth angular velocity
ϕ: spacecraft latitude
ψ: spacecraft heading angle

- **Passive to active oxidation limit**
  When the heat flux on the heat shield is particularly high and the atmospheric pressure is below a certain threshold, the shield material starts an oxidation process that increases significantly the surface temperature. This phenomenon leads to the erosion of the material which can be catastrophic. For a given heat shield it is necessary to find an empiric correlation between atmospheric pressure and heat fluxes, this way a passive to active oxidation curve can be calculated.

- **Maximum flight time**
  For thermal reasons, it might be necessary to set a maximum flight time. The heat shield radiates back into the atmosphere most of the heat absorbed but some of it flows through the shield itself via conduction. This conductive heat increases the temperature of the metallic structure underneath which can only withstand a maximum value, the structure heating increases with flight time, this is why there is a limit to it.

- **Maximum bank angle**
  The bank angle, which is the control parameter of the spacecraft, can be subject to a certain limit. As an example for IXV it is set to 90° in order to have a continuous connection with the GPS constellation.

- **Maximum bank angle rate**
  The spacecraft moments of inertia and the efficacy of the control surfaces (or the reaction control thrusters) determine the maximum bank angular velocity. The lower this angular rate is, the harder it is to control the vehicle. For IXV this limit is set to 12 deg/s.

- **No-fly zones**
  For geopolitical reasons or to avoid flying over populated areas it might be needed to define certain no-fly zones.

- **Ground station visibility**
  To guarantee a constant link between the vehicle and the ground segment it is necessary to ensure the visibility between the spacecraft and the ground stations.

2.3   Target

The aim of this thesis is to calculate and simulate a safe re-entry trajectory from the entry interface point to the Descent and Recovery System (DRS) deployment (which is the parachute used for the terminal part of the flight). The target conditions are necessary for a correct activation of the DRS, they are defined by four parameters:

- Target longitude

- Target latitude

- Target Mach number

- Target dynamic pressure

The goal of the GNC system is to enable a trajectory that allows a precise targeting of all these quantities while satisfying every constraint during descent.

2.4   Entry corridor

The Atmospheric re-entry problem represents a challenge in many fields, including the GNC field [4]. The vehicle must fly within a very specific region of space to survive the re-entry: at a given velocity if the spacecraft is flying in a region where the atmosphere is too dense it can be destroyed by the mechanical and thermal stresses. On the other hand, if it is flying where the atmosphere is too thin it loses control authority. This means that at any given velocity the re-entry vehicle must fly within a specific range of altitudes to survive and be controllable:
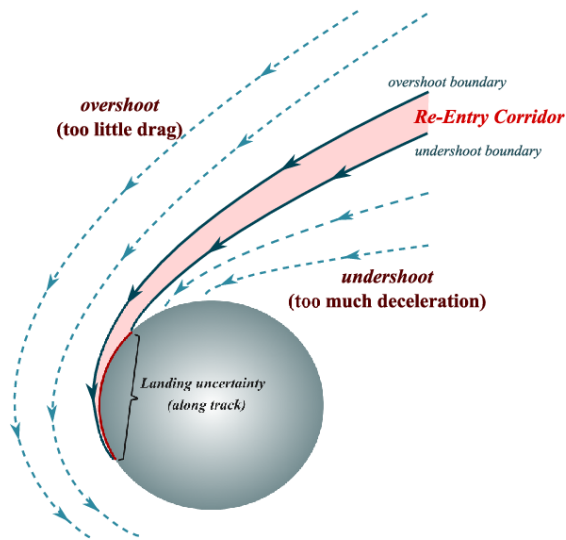
Figure 2.2: Qualitative visualization of the entry corridor

The entry corridor can be numerically calculated given some of the constraints introduced in section 2.2, specifically:

- Maximum dynamic pressure and stagnation point pressure

- Maximum load factor

- Maximum heat flux

- Maximum flap heat flux

- Ceiling limit

- Passive to active oxidation limit

10

The other constraints cannot be visualized in the entry corridor. A common representation of the entry corridor is drawn in the Altitude-Velocity (A-V) plane:
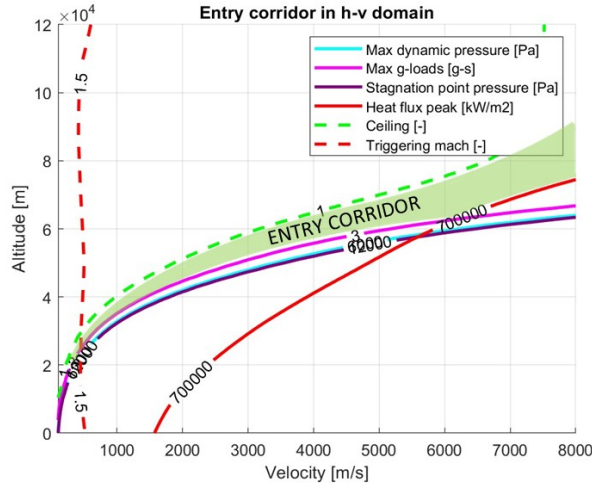
Figure 2.3: Entry corridor in the A-V plane

At high velocities the major danger is the heat flux that can reach critically high values, at lower velocities instead the limiting constraint becomes the G-load. The re-entry corridor can also be visualized in the Drag-Velocity (D-V) plane. This is the representation that will be utilized throughout this dissertation because it is more useful from a control point of view:
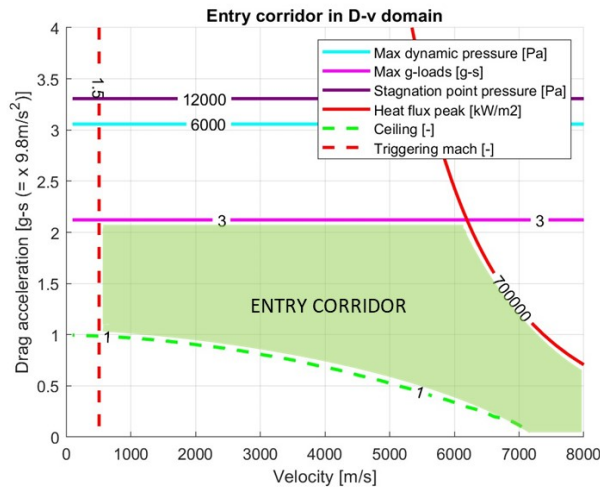
Figure 2.4: Entry corridor in the D-V plane

2.5   Vehicle dynamics

The model implemented in this study has three degrees of freedom (3-DoF), it considers the motion of the point mass located in the barycenter of the vehicle. The dynamical model is fully described by two vectorial equations of motion (or six scalar equations) derived directly by Newton second law [5]. In the Earth Centered Earth Fixed (ECEF) reference system (Earth centered and rotating coherently with the planet rotation) in cartesian coordinates, the system of equations can be written the following way:

$$
\begin{cases}
\frac{d\vec{r}}{dt} = \vec{v} \\
\frac{d\vec{v}}{dt} = \frac{\vec{L}}{m} + \frac{\vec{D}}{m} + \vec{g} - 2\vec{\Omega} \times \vec{v} - \vec{\Omega} \times \left(\vec{\Omega} \times \vec{r}\right)
\end{cases}
\tag{2.7}
$$

$\vec{r}$: radius vector
$\vec{v}$: velocity vector
$\vec{L}$: lift vector
$\vec{D}$: drag vector
$\vec{g}$: gravity vector
$\vec{\Omega}$: Earth angular velocity vector

The model used to propagate the trajectories integrates these equation in polar coordinates [6], the system is then translated in this form:

$$
\begin{cases}
\frac{dv}{dt} = -\frac{D}{m} - g\sin\gamma + \Omega^2 r \cos\phi \left(\cos\phi\sin\gamma - \cos\gamma\cos\psi\sin\phi\right) \\
\frac{dr}{dt} = v\sin\gamma \\
\frac{d\lambda}{dt} = \frac{v}{r}\cos\gamma\sin\psi/\cos\phi \\
\frac{d\phi}{dt} = \frac{v}{r}\cos\gamma\cos\psi \\
\frac{d\gamma}{dt} = \frac{L}{v}\cos\sigma + \left(\frac{v}{r} - \frac{g}{v}\right)\cos\gamma + 2\Omega\cos\phi\sin\psi + \\
\qquad + \frac{\Omega^2 r}{v}\cos\phi\left(\cos\phi\cos\gamma - \sin\gamma\cos\psi\sin\phi\right) \\
\frac{d\psi}{dt} = \frac{L\sin\sigma}{v\cos\gamma} + v\cos\gamma\sin\psi\tan\phi/r - 2\Omega\left(\tan\gamma\cos\phi\cos\psi - \sin\phi\right) \\
\qquad + \frac{\Omega^2 r}{v\cos\gamma}\sin\phi\cos\phi\sin\psi
\end{cases}
\tag{2.8}
$$

v: velocity
r: radius
λ: geocentric longitude
ϕ: geocentric latitude
γ: flight path angle
ψ: heading angle
σ: bank angle

Ω: Earth angular velocity
m: spacecraft mass
g: gravitational acceleration
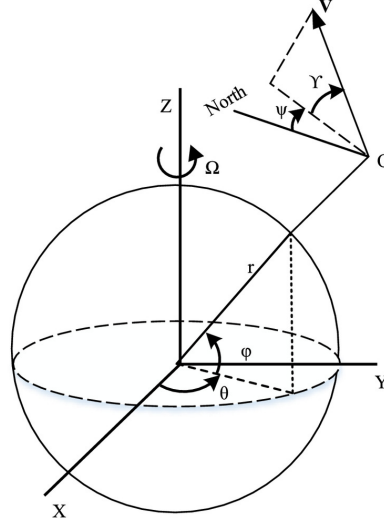
Figure 2.5: Angles in ECEF coordinates

The Lift and Drag aerodynamic forces are calculated the following way:

$$L = \frac{1}{2}\rho(h)v^2 S C_l(M, \alpha) \qquad (2.9)$$

$$D = \frac{1}{2}\rho(h)v^2 S C_d(M, \alpha) \qquad (2.10)$$

The aerodynamic coefficients C_l and C_d are mostly a function of Mach number and angle of attack, the angle of attack is usually itself a function of the Mach number since the vehicle has to follow a certain trim line to ensure aerodynamic stability at every Mach regime. The model described in this thesis also uses an advanced aerodynamic database developed for IXV and SpaceRider vehicles, in this case the aerodynamic coefficients are function of: Mach number, AoA, dynamic pressure, pressure, temperature, side-slip angle and uncertainties.

The Atmospheric model utilized was developed for the IXV flight, it contains also uncertainties which will be used in the Montecarlo analysis. The gravity model is simply spherical.

13

2.6 IXV entry vehicle

IXV or Intermediate eXperimental Vehicle is a European experiment that demonstrated and validated the re-entry technologies [7]. It is a lifting body vehicle with a length of 5.5 meters, a width of 2.2 meters and a height of 1.5 meters. Its shape is the result of a set of requirements such as the maximization of the internal space for experiments.

IXV control authority is given by reaction control thrusters while in space and by aerodynamic surfaces during the atmospheric phase. The re-entry is divided in two parts: the first one takes place from EIP to DRS activation (the supersonic parachute deployment) and it is actively controlled; the second part, from DRS activation to splashdown, is not controlled and the vehicle is drifted by the winds.

The vehicle was successfully launched one time in 2015 by a Vega rocket in Kourou (French Guiana). The launcher set IXV in a nearly equatorial suborbital trajectory with an apogee of around 450 *km*, when the vehicle reached the EIP it started the atmospheric re-entry phase flying more than 7000 *km* downrange in about 20 minutes. Then it safely landed in the pacific ocean and was recovered by a ship.

Every constraint and boundary condition relative to IXV flight has been used in the development of this thesis in order to simulate a realistic scenario.
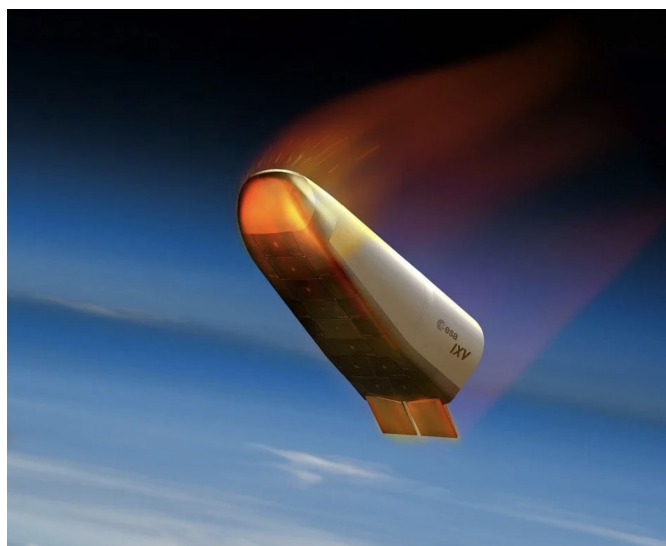
Figure 2.6: Intermediate eXperimental Vehicle

Chapter 3

Optimization overview

The following chapter will discuss the general concept of optimization [8] with the different strategies known today. In the case of this thesis a specific application of the black box optimization approach has been adopted, which will be described in more detail throughout the chapter.

3.1 General concept of optimization

Optimizing is finding the best solution to a given problem by manipulating a set of controllable variables which are usually subject to certain constraints. The concept of optimization is inherent in nature and it is the goal of the evolutionary process: we can think about the shape of beehives that maximizes the volume of honey contained, the evolution of the human hand that allow us to manipulate an enormous quantity of tools with great precision, or the shape of bird wings that changes and optimizes itself for the different flight conditions. This concept can be applied also to engineering and there are mathematical tools able to solve a variety of optimization problems. A few of these problems can be solved in a closed form such as the brachistochrone problem, but most of them can only be solved numerically.

There are two main classes of optimization problems, "finite-dimensional" and "infinite-dimensional" problems:

- A finite-dimensional problem is for example the packing optimization issue, only a finite number of real variables are involved such as the position and the orientation of the thrusters.

- An infinite-dimensional problem is the low-thrust trajectory optimization, where the control and trajectory functions are unknown.

The field of trajectory optimization has a rich and captivating history. The problem can be defined as finding a trajectory that fulfil certain initial and final conditions while satisfying a set of constraints Q and minimizing a given cost function J. The goal could be that of minimizing the propellant consumption or the overall control inputs. It might be necessary to define upper and lower bounds ($\overline{U}$ and $\underline{U}$) to the control variables u, in the specific case of atmospheric re-entry the spacecraft is subject to a maximum allowed bank angle value and a maximum bank angle rate due to the vehicle inertia and the efficacy of the actuators.

The generic optimization paradigm, in finite dimension, can be defined as follows:

$$\begin{cases} min \ J(u) \\ Q(u) \leq 0 \\ \underline{U} \leq u \leq \overline{U} \end{cases} \quad \text{with} \quad \begin{cases} u \in R^n \\ J: \ R^n \to R \\ Q: \ R^n \to R^m \end{cases} \tag{3.1}$$

Another important characteristic of optimization problems is whether they are convex or non convex. Convex problems are much easier to solve because they enable efficient line search and a local optimization algorithm is sufficient since the local solution coincides with the global solution. For non convex optimization problems a global optimization algorithm is necessary to ensure that the local solution found is also the global solution [9]. Unfortunately the trajectory optimization problem is non-linear and non-convex. in the context of this thesis Matlab Global Optimization Toolbox was utilized to approach the non-convexity of the problem [10]. The specific algorithm utilized is the Sequential Quadratic Programming, specialized for non-linear problems.
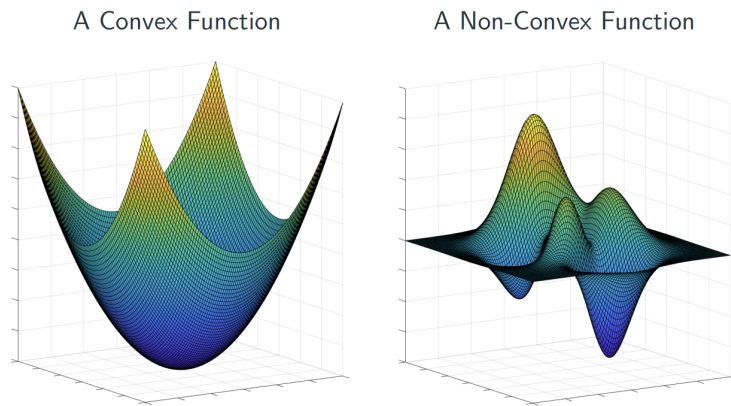
Figure 3.1: Convex vs non convex functions

There are many different types of optimal control problems but in each one of them the following elements must be defined:

- The mathematical model of the controlled system and the environment surrounding it.

- The declaration of the performance index or cost function.

- The declaration of every constraint and boundary condition that must be satisfied by the state vector of the system and the control inputs.

Fortunately, various methods exist today to tackle real-world optimization problems. They can be classified into three main categories:

- **Direct methods**
  These use discretization to transform the optimal control problem into a finite-dimensional nonlinear programming (NLP) problem which is solved directly [11]. In the traditional approach the trajectory is usually subdivided into N intervals, state and control variables are considered constant in each interval, resulting in a large-scale problem. Direct methods offer the advantage of accommodating almost any problem formulation and they are robust: the algorithm performs well under many different initial conditions and boundaries. On the downside, compared to indirect methods, they can be computationally expensive and relatively less accurate.

- **Indirect methods**
  Here the problem is considered continuous for both state and control variables, the necessary (and sufficient) conditions for optimality, given by Pontryagin Maximum Principle (PMP), are used to solve the optimal control problem in terms of a Boundary Value Problem (BVP). The trajectory may be divided into arcs in the presence of discontinuities or changes in the differential equations used. The problem modeled with an indirect method is generally smaller and with fewer parameters to evaluate, this results in shorter computational times and potentially higher accuracy compared to direct methods. However, it is necessary to determine the costates, which lack physical meaning and it can be challenging to calculate them in order to satisfy all constraints and boundaries of the problem. Inadequate selection of these variables can hinder algorithm convergence or lead to numerical issues.

- **Evolutionary algorithms**
  These employ mechanisms inspired by nature, the problems are solved by emulating the behavior of living organisms, specifically the concepts of Darwinian Evolution. The approach is the following: the initial guess solutions are randomly generated and subsequently their effectiveness is evaluated. The best

solutions are then selected for reproduction and undergo mutation, generating improved solutions throughout an iterative process. Various techniques can be employed to achieve the desired result, the Genetic Algorithms are the most used.

3.2 Black box optimization

Black Box Optimization (BBO) [12] can be used when the structure of the objective function J or the constraint function Q is unknown, non-existent, or lacks an analytic expression. The BBO approach is frequently used when the objective and/or constraint function require the execution of a computer simulation such as a trajectory propagation (like in the case of this thesis). Another less frequent case is when the output is an experimental result and thus cannot be modeled analytically. The BBO approach is used in many different contexts such as material science, computer engineering design, road design optimization, cardiovascular geometries. Not many applications can be found in the field of trajectory optimization.

The general scheme of the BBO optimization is the following: the optimization parameters u are the inputs for the black-box function, they must be contained within an upper bound $\overline{U}$ and a lower bound $\underline{U}$. The black-box function performs the computer simulation and formulates the output vector y:

$$\begin{cases} y = f(u) \\ \underline{U} \leq u \leq \overline{U} \end{cases} \tag{3.2}$$

The output y and the optimization parameters u are then used to calculate the cost function J and the constraint function Q:

$$J(u,y) \quad \text{s.t.} \quad \begin{cases} \underline{U} \leq u \leq \overline{U} \\ Q(u,y) \leq 0 \end{cases} \tag{3.3}$$

The values of J and Q are then used by the optimization algorithm to calculate the next values of u. This BBO approach is used with a direct optimization method, figure 3.2 shows the BBO block diagram:

- u: optimization variables
- f: black box function
- y: output vector of the simulation
- J: cost function
- Q: additional constraints function

SIMULATION PART

BLACK BOX SIMULATION

$$\begin{cases} y = f(u) \\ \underline{U} \leq u \leq \overline{U} \end{cases}$$

new simulation
output y

OPTIMIZER

$$min\big(J(u,y)\big)$$
$$s.t.$$
$$\begin{cases} \underline{U} \leq u \leq \overline{U} \\ Q(u,y) \leq 0 \end{cases}$$

new u
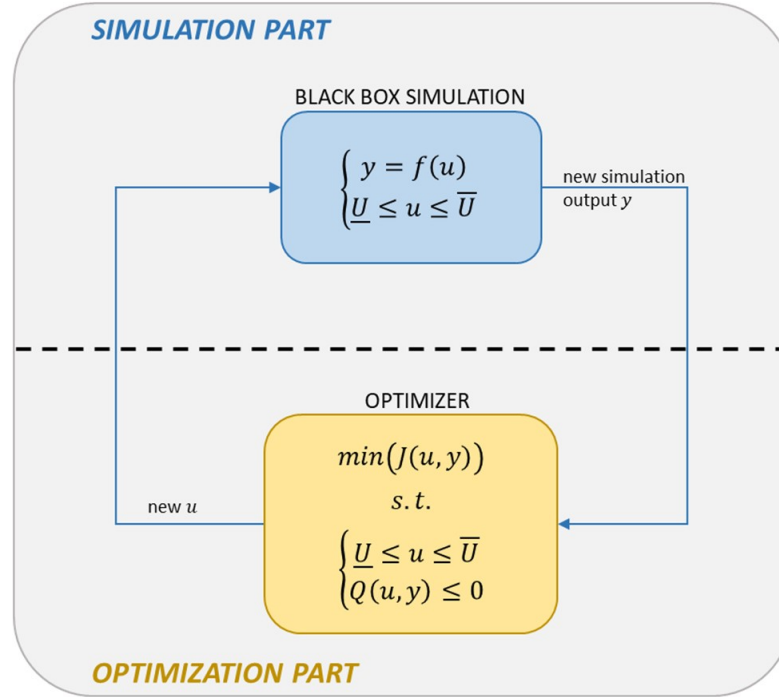
OPTIMIZATION PART

Figure 3.2: Black box optimization block diagram

In a traditional direct approach there are hundreds or thousands of optimization variables depending on the precision of the trajectory discretization, and there are a similar number of constraints. By using the BBO approach the number of optimization variables is greatly reduced (10 at most, in the case of this thesis) and the majority of the constraints are satisfied inside the black-box function itself.

The atmospheric re-entry problem is not defined by a clear and obvious objective function (there is no propellant consumption to be minimized), for this reason the cost function can be properly chosen. In the approach here followed, the cost function has been defined as a weighted sum of different errors associated with each constraint. This problem is actually of a feasibility type: when the selected objective function is minimized the problem feasibility has been obtained. The intrinsic feasibility of the problem makes the optimization model very fast: the only goal of the optimization algorithm is to minimize the cost function and it does

not have to look for a feasibility region beforehand.

The details of the different optimization models developed in this thesis will be described in chapters 5 and 6.

3.3   Sequential Quadratic Programming

Sequential Quadratic Programming (SQP) [13] is an iterative optimization algorithm specialized in solving constrained non-linear optimization problems. It can be considered a quasi-Newton method. It is one of the most successful algorithms used in the space industry and it has proven to be the fastest even for the work presented in this thesis.

This algorithm can handle a high degree of non-linearity but it incorporates the calculation of many derivatives. For this reason the objective and constraint functions need to be at least twice differentiable (everywhere). the SQP method solves a set of optimization subproblems, each one of them optimizes a quadratic model of the cost where the constraints are linearized.

If the problem is unconstrained (which is the case for most of the models developed in this thesis), the algorithm is reduced to Newton method.

Chapter 4

Guidance and Control solutions

This chapter describes in detail the guidance and control algorithms developed in this thesis. The GNC system goal is to guide and control the vehicle allowing it to follow a predetermined optimal reference trajectory in order to survive re-entry. The control parameter is traditionally just one, the bank angle, which can be modulated via aerodynamic surfaces (as in the case of space shuttle or IXV entry vehicle) or reaction control thrusters (like the dragon capsule).

4.1   Reference trajectory

The guidance and control system has to follow with high accuracy a given reference trajectory obtained through an optimization process. This reference trajectory is located within the entry corridor boundaries and satisfies every constraint, including the ones that are not directly visible in the entry corridor itself such as integral heat flux, maximum flight time, geographical constraints... From the reference trajectory are derived a set of three different profiles needed by the feedback control loop of the GNC system. The first profile can be plotted in the Drag-Velocity plane [14]:
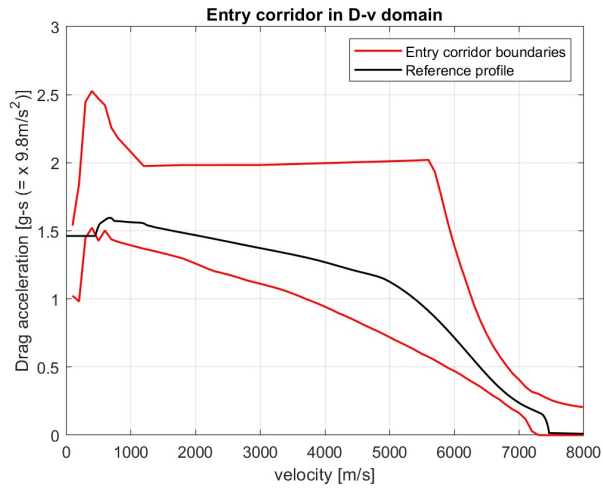
Figure 4.1: Drag-Velocity reference profile

The control system must accurately follow the D-V reference profile in order to stay within the entry corridor boundaries.

The second profile is plotted in the Energy-Range plane:
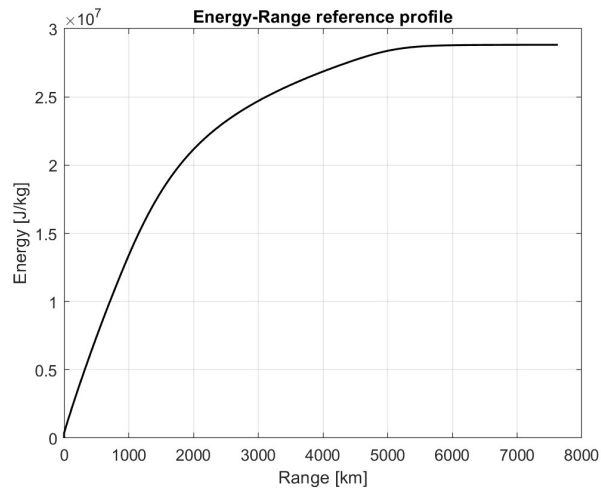
Figure 4.2: Energy-Range reference profile

The energy is calculated as the sum of kinetic and potential energy per unit mass of the spacecraft at a given distance from the target:

$$E = \frac{1}{2}v^2 + g_0 h \tag{4.1}$$

The Energy-Range profile is needed by the guidance algorithm to adjust the Drag-Velocity reference profile: this is necessary in order to reach the target with the right amount of energy in terms of altitude and velocity of the spacecraft. This will be discussed with more detail in section 4.3.

Finally the third profile can be plotted in the Altitude-Range plane:
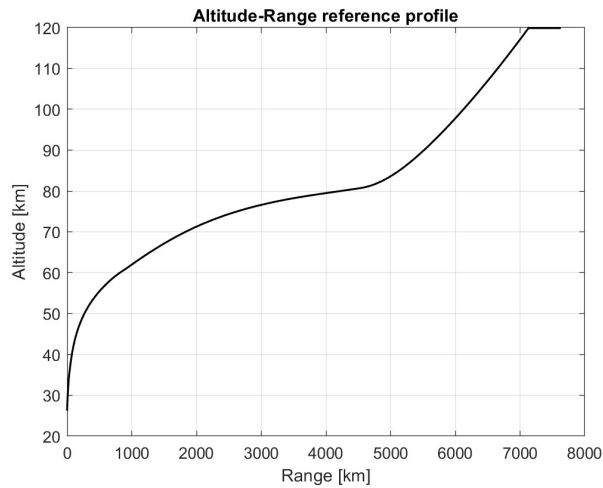
Figure 4.3: Altitude-Range reference profile

This profile can by used by the guidance algorithm as an alternative to the Energy-Range profile to achieve the same goal: the adjustment of the reference trajectory in the D-V plane. During the development of the model better performances were obtained using the Energy-Range profile instead of the Altitude-Range, for this reason from now on this last profile will not be mentioned.

4.2   Control parameter: bank angle

The feedback control law must follow the D-V reference profile by controlling the lift generated by the spacecraft. This action can be achieved in two ways:

- The variation of the angle of attack, which modulates the magnitude of the lift vector

- The variation of the bank angle, which changes the direction of the lift vector and consequently modulates its vertical component

The first strategy is not used traditionally: as said in section 2.5 the vehicle has to follow a certain AoA profile during re-entry due to aerodynamic stability reasons. This means that the only real control parameter is the bank angle, which indicates the rotation of the lift vector around the velocity vector axis:
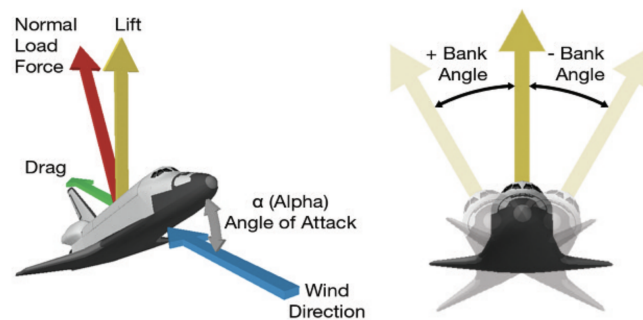
Figure 4.4: Bank angle and angle of attack representation

There is a major drawback to this kind of control: by rotating the lift vector an horizontal lift component is created which determines a drift of the trajectory to the left and to the right depending on the bank angle sign. To counteract this phenomenon a series of bank reversal manoeuvres are needed, where the bank angle changes in sign but not in magnitude. This will be discussed in more detail later.
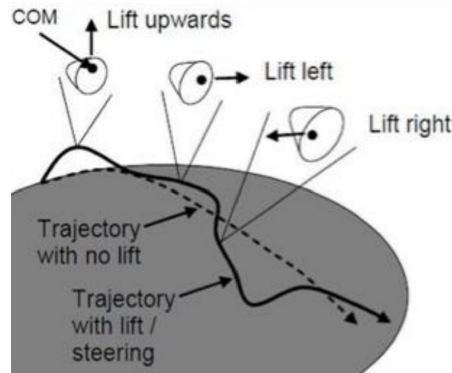
Figure 4.5: Bank control drift

4.3 Guidance logic for energy management

As anticipated in section 4.1, an important goal of the GNC system is to deliver the vehicle to the target with the right amount of energy, in other words the spacecraft must have the right velocity and altitude for DRS activation when it reaches the target position. To ensure this happens correctly a guidance law must be implemented.

The input for this guidance law is the error between the measured energy and the reference energy at a given distance from the target. Then the guidance algorithm calculates a corrective action to reduce this error:

- If the actual energy is higher than the reference, the guidance law scales up the D-V reference profile to higher drag values to dissipate the excessive energy.

- If the actual energy is lower than the reference, the guidance law scales down the D-V reference profile to lower drag values to limit energy dissipation.

The following lines describe this guidance law. Firstly the energy error is calculated:

$$e = \frac{E - E_{ref}(range)}{E_{ref}(range)} \tag{4.2}$$

E: actual energy
E_{ref}: reference energy

Then this error and its first derivative are used in a PD-like guidance law to adjust the D-V reference profile:

$$\underline{D_{ref}(v)} = \overline{D_{ref}(v)} \cdot \left(1 + K_1 e + K_2 \frac{de}{dt}\right) \tag{4.3}$$

$D_{ref}(v)$: adjusted reference drag
$\overline{D_{ref}(v)}$: reference drag
K_1: proportional gain
K_2: derivative gain

Finally the adjusted reference drag is saturated whenever it exceeds a maximum threshold safety value, this is done to ensure that the reference drag always lays within the entry corridor margins:

$$\begin{cases} \overline{D_{ref}(v)} = \underline{D_{ref}(v)} & \text{if } \underline{D_{ref}(v)} < D_{safe} \\[2mm] \overline{D_{ref}(v)} = D_{safe} & \text{if } \underline{D_{ref}(v)} > D_{safe} \end{cases} \tag{4.4}$$

$\overline{D_{ref}(v)}$: adjusted and saturated reference drag
D_{safe}: maximum safety drag

4.4 Control law

The aim of the control law is to calculate an optimal control lift to follow with high accuracy the D-V reference profile. This lift is then translated into a bank angle value. The algorithm developed in this thesis calculates the control lift as the sum of three terms that will be described in the following subsections.

4.4.1 Commanded lift

The commanded lift is calculated from the error between the reference drag and the actual measured drag, this error is expressed the following way:

$$e = D - \overline{D_{ref}(v)} \tag{4.5}$$

This error, its first derivative and its integral are then used in a PID-like control law which calculates the desired lift. There are other terms besides the classic PID terms that will be discussed in more detail later:

$$L_c = \frac{K_q}{q} \cdot \left(K_p e + K_d \frac{de}{dt} + K_i \int_0^t e\, dt + \overline{K_h(v)} \frac{dh}{dt} \right) \tag{4.6}$$

$$\overline{K_h(v)} = \begin{cases} 0 & \text{if } v < 5000 m/s \\ -K_h \cdot \frac{v-5000}{10000-5000} & \text{if } v > 5000 m/s \end{cases} \tag{4.7}$$

K_p: proportional gain
K_d: derivative gain
K_i: integrative gain
K_h: vertical velocity gain
K_q: dynamic pressure gain

There are two more terms other than the classic PID terms:

- The $\overline{K_h(v)}\frac{dh}{dt}$ term proved to be useful in attenuating oscillations in the first part of re-entry at very high altitudes and velocities, but harmful at low velocities because it does not allow for a precise matching of the reference profile. For this reason the gain $\overline{K_h(v)}$ decreases linearly until a velocity of 5000 *m/s* and then it becomes null. The value of 5000 *m/s* is chosen by trial and error and it is not necessarily the best one, it could be improved through an optimization process.

- The whole expression is multiplied by $\frac{K_q}{q}$, this terms is big at low dynamic pressures and small at high dynamic pressures. The idea is to increase the gains when the aerodynamic forces are small and the vehicle loses control authority, and to decrease them when the aerodynamic forces are sufficiently high for the vehicle to have great control authority.

4.4.2   Equilibrium glide lift

The equilibrium glide lift by itself allows the vehicle to fly with zero vertical acceleration because the sum of the vertical forces acting on it (weight, lift and centrifugal) equals zero. The implementation of this term in the control law creates a symmetry on the effectiveness of the commanded lift described in the section 4.4.1. For a given error measured between the reference drag and the actual drag, called e_0, the commanded lift is the same whether the error is positive or negative aside from the sign: $|L_c(e_0)| = |L_c(-e_0)|$. Without the use of the equilibrium glide lift, if the error is negative the vertical forces acting on the spacecraft are $F_- = L_c(-e_0) - weight + centrifugal$, if the error is positive the forces are $F_+ = L_c(e_0) - weight + centrifugal$. It is obvious that there is no symmetry in these two cases because $|F_-| \neq |F_+|$: the control action is

more effective when the vehicle has to fly at lower altitudes and less effective when it has to fly at higher altitudes. By introducing the equilibrium glide lift the weight and the centrifugal forces are already counteracted and the symmetry is restored: $F_- = L_c(-e_0) + L_0 - weight + centrifugal = L_c(-e_0)$ and $F_+ = L_c(e_0) + L_0 - weight + centrifugal = L_c(e_0)$ so that $|F_-| = |F_+|$.

The equilibrium glide lift can be expressed the following way:

$$L_0 = m \cdot \left(\left(g - \frac{v^2}{r} \right) \cos \gamma - 2\Omega v \cos \phi \sin \psi - \Omega^2 r \cos \phi \left(\cos \gamma \cos \phi + \cos \psi \sin \gamma \sin \phi \right) \right) \quad (4.8)$$

4.4.3 Safety lift

This term is introduced as a safety measure to ensure that the boundaries of the entry corridor are not surpassed. Firstly the error between the actual drag and the drag corresponding to the entry corridor boundary (called D_{max}) is calculated:

$$e = D_{max} - D \quad (4.9)$$

Secondly this error is used to compute the safety lift:

$$L_s = \frac{1}{(e/0{,}1)^{100}} \quad (4.10)$$

The value of L_s is basically zero if the error is bigger than 0,1. When the spacecraft is close to the corridor upper boundary (in the D-V plane) and the error becomes smaller than 0,1 the value of L_s grows exponentially commanding the vehicle to move to higher altitudes.

4.4.4 From lift to bank angle

The ultimate control lift is the sum of the three terms described before:

$$L_{control} = L_0 + L_c + L_s \quad (4.11)$$

This control lift is translated into a bank angle command with the following expression:

$$\sigma = \arccos \left(\frac{L_{control}}{L \cos \gamma} \right) \quad (4.12)$$
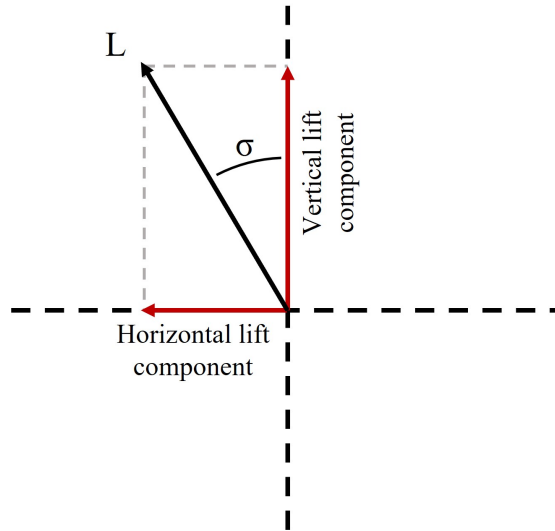
Figure 4.6: Bank angle and lift components

4.5   Guidance logic for bank reversal

Bank reversal manoeuvres are necessary to compensate the lateral drift deriving from the horizontal lift component. The logic is very simple, firstly the angle between the velocity vector and the target vector (heading error) is calculated:

$$\alpha = bearing - heading \tag{4.13}$$

The heading error must stay within a maximum and a minimum value which define a heading error corridor. Each time α reaches the maximum or the minimum boundary, a bank reversal manoeuvre is commanded:

$$sign = \begin{cases} 1 & \text{if } \alpha > \alpha_{max} \\ -1 & \text{if } \alpha < -\alpha_{max} \\ sign_{old} & \text{if } -\alpha_{max} < \alpha < \alpha_{max} \end{cases} \tag{4.14}$$

$$\overline{\sigma} = sign \cdot \sigma \tag{4.15}$$

Figure 4.7: The heading error α

Figure 4.8: Heading error corridor

The frequency of bank reversal manoeuvres increases as the vehicle gets closer to the target.
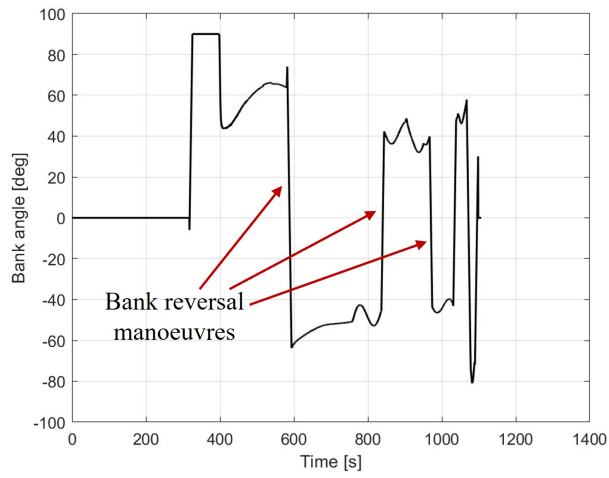
Figure 4.9: Bank profile with reversals

A simplified block diagram of the guidance and control subsystem is shown in figure 4.10:
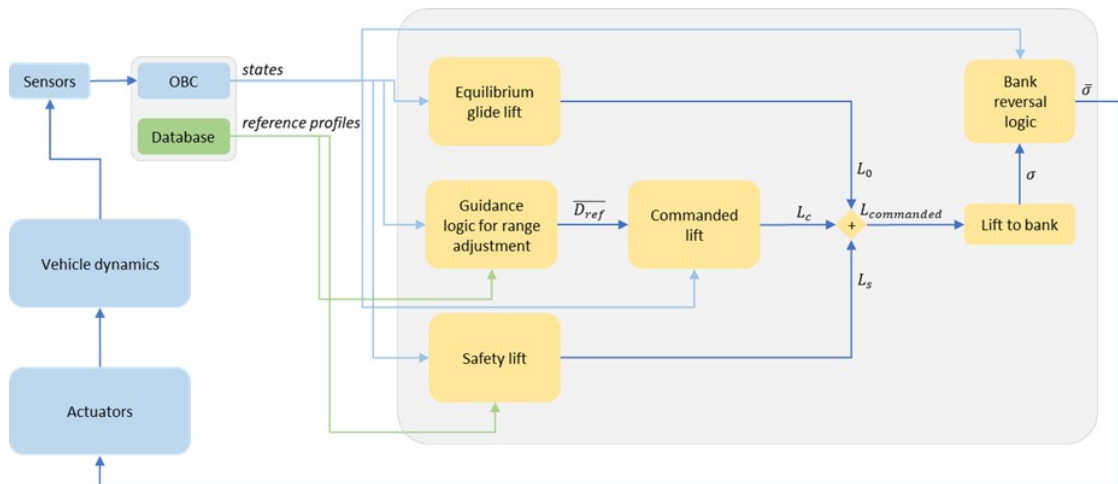
Figure 4.10: Guidance and control block diagram

Chapter 5

Variable entry interface point tool

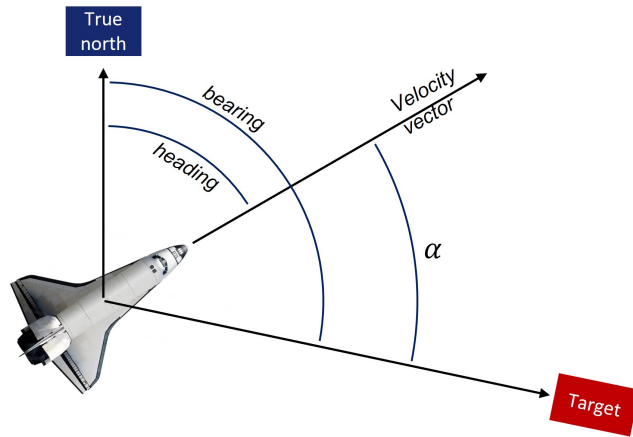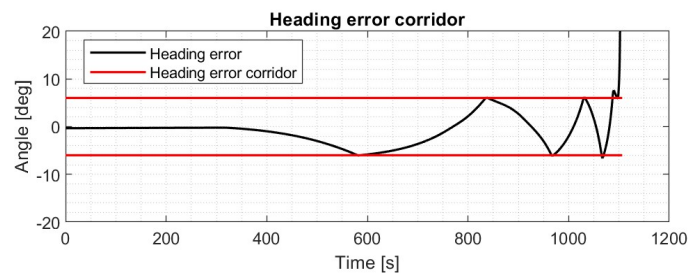This chapter will discuss in detail the optimization process developed to obtain reference trajectories that satisfy every constraint discussed in chapter 2. The target position and conditions are known but the EIP is not fixed: the tool calculates the best entry interface point.

The tool is divided into many parts which will be described in the sections of this chapter.

5.1   Model inputs

The tool needs several inputs to operate:

- **Atmospheric model**
  The atmospheric model must be loaded in the form of a matrix with three columns: the first column is the altitude vector, the second column is the density vector and the third column is the speed of sound vector.

- **Aerodynamic coefficients**
  The aerodynamic coefficients are expressed as a function of Mach number, they must be loaded in a matrix with three lines: the first line is the Mach number vector, the second line is the lift coefficients vector and the third line is the drag coefficients vector.

- **Spacecraft constants**
  The model needs to know the mass of the vehicle, the surface area, the nose radius, and other quantities which are only used for the entry corridor

calculation: the catalytic coefficient, the elevon and aileron deflections and the angle of side-slip.

- **Orbital parameters**
  The original orbit where the spacecraft flew before re-entry must be known in order to correctly calculate the EIP conditions. This model considers only circular orbits and the inputs needed are just the inclination and the semi-major axis. Here the user also chooses if the goal is for the vehicle to fly to the target while moving towards the ascending node or the descending node of the orbit.

- **EIP conditions**
  In this section the user sets the EIP altitude and flight path angle, these inputs together with the known orbital parameters allow for the calculation of the other quantities of the EIP state vector: initial velocity, longitude, latitude and heading angle. The user also chooses a minimum and a maximum range from EIP to target: the actual entry interface point chosen by the model will be located within these boundaries.

- **Target conditions**
  The necessary target conditions are: final longitude, final latitude, final Mach number and final dynamic pressure.

- **Ground stations**
  The user must insert the information about the ground stations in a matrix where each line represents a different station. The first two elements of each line are the longitude and latitude of the station, the third element is its altitude, the fourth element is the minimum elevation at which a communication link can be created, and finally the fifth element is the minimum desired visibility window (in terms of duration) between the station and the spacecraft. This section can be left empty if no ground stations are implemented.

- **Constraints**
  In this section the following constraints are defined: maximum dynamic pressure, maximum pressure at stagnation point, maximum load factor, maximum heat flux, maximum heat flux on the flaps, ceiling value, maximum integral heat flux, flight time, maximum bank angle and maximum bank angle rate.

- **Heading error corridor**
  The user must insert four different values of maximum heading error that will define a heading error corridor as function of the distance from target:

$$\alpha_{max} = \begin{cases} \alpha_1 & \text{if range} > 3500km \\ \alpha_2 & \text{if } 3500km > \text{range} > 1500km \\ \alpha_3 & \text{if } 1500km > \text{range} > 500km \\ \alpha_4 & \text{if range} < 500km \end{cases} \tag{5.1}$$

5.2 EIP conditions map

As anticipated before, the tool calculates the optimal EIP location. The minimum and maximum EIP distances from the target are chosen by the user. The length between these two extremes is then divided into many equidistant points and the EIP conditions are calculated in every point. The actual EIP location is then interpolated between these points. It is therefore necessary to calculate a map of feasible EIP conditions for the model to interpolate.

5.2.1 Orbit RAAN determination

The reentry is only possible if the ground track of the spacecraft orbiting Earth intersects the target location, or at least passes very close to it. This means that not every orbit can be used for re-entry and it is necessary to wait until this condition is satisfied:
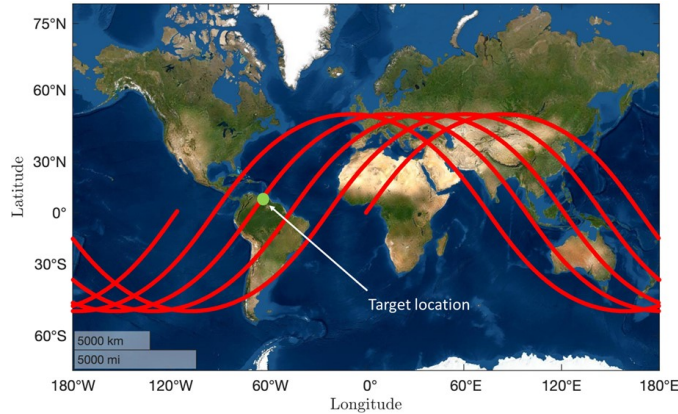
Figure 5.1: Ground track of multiple orbits

In this thesis instead of waiting for the proper orbit that allows re-entry, the Right Ascension of the Ascending Node (RAAN) is chosen in order to geometrically

satisfy the necessary intersection condition between target and ground track. In reality the orbit RAAN is known but choosing it in order to satisfy this condition does not change the physics of the problem at all, that is why it is implemented this way.

The RAAN is calculated analytically using the geometrical relations of spherical right triangles. There are eight different expressions depending on three parameters: the target latitude (northern or southern hemisphere), the inclination of the orbit (prograde or retrograde) and the part of the orbit where the re-entry takes place (ascending node side or descending node side). For example in the following case: target in the northern hemisphere, prograde orbit and descending node side, the expression is the following:

$$a = \frac{\pi}{2} - \arccos\left(\cot\left(i\right)\cot\left(\frac{\pi}{2} - L\right)\right) \tag{5.2}$$

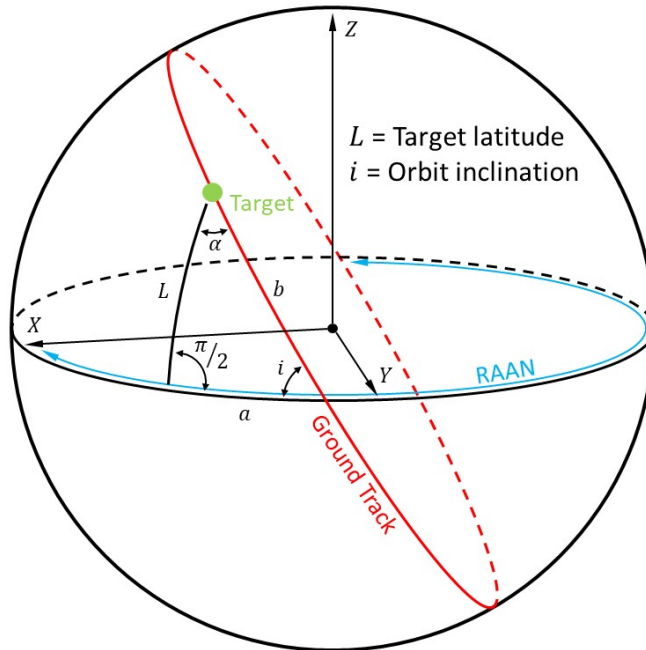$$RAAN = Longitude_{target} + a + \pi \tag{5.3}$$

Figure 5.2: Spherical geometry relations

5.2.2   Calculation of EIP conditions

The spacecraft orbiting the Earth in order to re-enter atmosphere has to perform an entry burn to reduce its energy and lower its perigee. This ΔV is applied in the opposite direction relative to the velocity vector of the vehicle. The EIP conditions uniquely depend on the modulus of this ΔV, on the true anomaly value ν where the ΔV is applied and on the time of flight T after the entry burn:
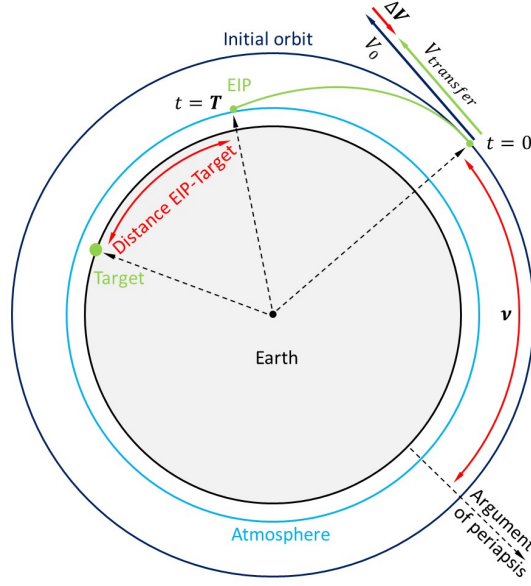
Figure 5.3: EIP as function of ΔV, ν and T

Calculating the correct ΔV, ν and T to get the desired EIP flight path angle, altitude and range from target is not an easy task because Earth is an ellipsoid: by changing ν, also ΔV and T have to change to get the desired flight path angle, and it is very easy to miss completely the atmosphere since this angle is so small.

After many attempts and algorithms the best solution for this problem is to develop an optimization model whose optimization parameters are ΔV, ν and T, and the cost function minimizes the error between the actual EIP conditions and the desired EIP conditions:

$$\begin{cases} J_1 = ((\overline{range_{EIP}} - range_{EIP}) \cdot 10^{-6})^2 \\ J_2 = \left(\left(\overline{fpa_{EIP}} - fpa_{EIP}\right) \cdot 10^2\right)^2 \\ J_3 = \left(\left(\overline{H_{EIP}} - H_{EIP}\right) \cdot 10^{-5}\right)^2 \\ J = J_1 + J_2 + J_3 \end{cases} \tag{5.4}$$

36

$\overline{range_{EIP}}$: desired distance EIP-target
$\overline{fpa_{EIP}}$: desired EIP flight path angle
$\overline{H_{EIP}}$: desired EIP altitude

J_1 relates to the error between the desired EIP position and the actual EIP position, J_2 indicates the error between the desired and actual EIP flight path angle and J_3 represents the error between the desired and actual EIP altitude. J is the sum of these three terms to be minimized.

The optimization model uses the black-box approach: every constraint is taken into account inside the trajectory propagator (which is the black-box) and there are no additional constraints that need to be verified. This means that the optimizer has to solve a problem which is always feasible and for this reason it always converges to a solution.

- u: optimization variables
- f: black box function
- y: output vector of the simulation
- J: cost function

SIMULATION PART

BLACK BOX SIMULATION

$$\begin{cases} y = f(u) \\ \underline{U} \le u \le \overline{U} \end{cases}$$

$y = [range_{EIP} \quad fpa_{EIP} \quad H_{EIP}]$

OPTIMIZER

$$min(J(y))$$
$$s.t.$$
$$\underline{U} \le u \le \overline{U}$$

$u = [\Delta V \quad \nu \quad T]$
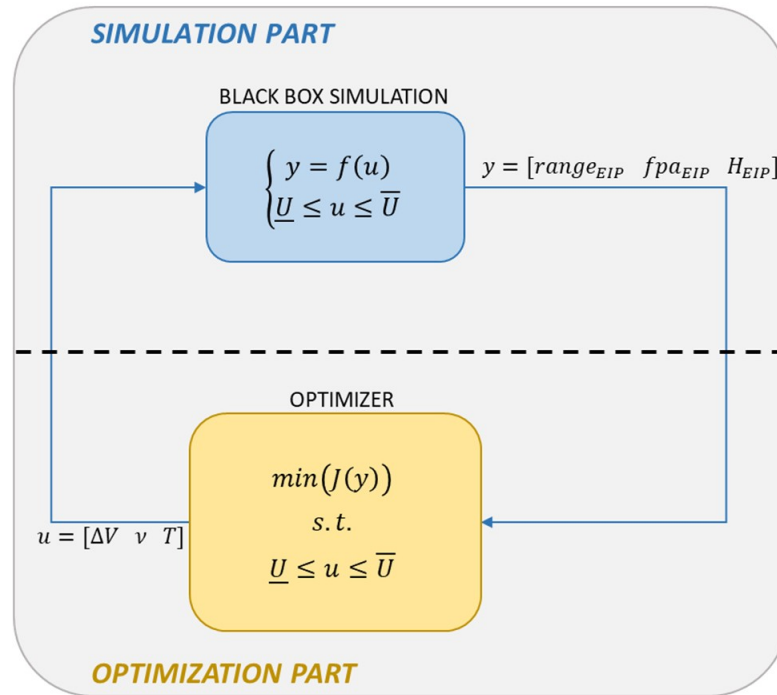
OPTIMIZATION PART

Figure 5.4: EIP conditions optimization model

The optimization algorithm is *Interior-point*; the function used to integrate the equations of motion is *ode89*, which is a 8th order variable step Runge-Kutta method for non stiff problems.

The process is extremely fast: the model finds the solution in 3 or 4 seconds and the desired values are obtained with very high accuracy. This model is run 20 times in order to calculate the EIP conditions in 20 equally spaced locations ranging from the minimum and the maximum distances EIP-target chosen by the user in section 5.1. For each run the whole state vector is saved (longitude, latitude, velocity, radius, flight path angle and heading angle) together with the values of ΔV, ν and T. This creates the EIP conditions map:

		1	2	3	4	5	6	7	8	9	10
Velocity	[m/s]	7429,3	7429,3	7429,3	7429,3	7429,3	7429,3	7429,3	7429,3	7429,3	7429,4
Radius	[m]	6498137	6498137	6498137	6498137	6498137	6498137	6498137	6498137	6498137	6498137
Longitude	[rad]	3,509	3,443	3,378	3,312	3,246	3,180	3,115	3,049	2,983	2,917
Latitude	[rad]	-0,002	-0,009	-0,015	-0,022	-0,028	-0,035	-0,041	-0,047	-0,053	-0,058
Flight path	[rad]	-0,021	-0,021	-0,021	-0,021	-0,021	-0,021	-0,021	-0,021	-0,021	-0,021
Heading	[rad]	1,470	1,470	1,471	1,473	1,475	1,477	1,480	1,483	1,487	1,491
Range to Target	[m]	4000000	4421052	4842105	5263158	5684210	6105263	6526316	6947368	7368421	7789474
True anomaly	[rad]	2,951	3,021	3,092	3,163	3,233	3,304	3,375	3,445	3,516	3,587
DV	[m/s]	-102,40	-102,39	-102,38	-102,38	-102,37	-102,37	-102,37	-102,36	-102,36	-102,36
T	[s]	1974	1974	1975	1975	1975	1975	1975	1975	1975	1975

|		11	12	13	14	15	16	17	18	19	20
Velocity	[m/s]	7429,4	7429,4	7429,4	7429,4	7429,4	7429,4	7429,4	7429,4	7429,4	7429,4
Radius	[m]	6498137	6498137	6498137	6498137	6498137	6498137	6498137	6498137	6498137	6498137
Longitude	[rad]	2,851	2,785	2,719	2,653	2,587	2,521	2,455	2,388	2,322	2,256
Latitude	[rad]	-0,063	-0,068	-0,073	-0,077	-0,081	-0,084	-0,087	-0,090	-0,092	-0,093
Flight path	[rad]	-0,021	-0,021	-0,021	-0,021	-0,021	-0,021	-0,021	-0,021	-0,021	-0,021
Heading	[rad]	1,495	1,500	1,505	1,511	1,517	1,523	1,529	1,536	1,543	1,550
Range to Target	[m]	8210526	8631579	9052631	9473684	9894737	10315789	10736842	11157895	11578947	12000000
True anomaly	[rad]	3,657	3,728	3,799	3,869	3,940	4,010	4,081	4,151	4,222	4,292
DV	[m/s]	-102,37	-102,37	-102,37	-102,38	-102,38	-102,39	-102,40	-102,40	-102,41	-102,42
T	[s]	1975	1975	1975	1975	1975	1975	1975	1975	1975	1975

Figure 5.5: EIP conditions map

5.3 Entry corridor definition

In this section the entry corridor is calculated using the equations defined in section 2.2. The constraints taken into account for the definition of the entry corridor are listed in section 2.4. Figure 5.6 shows the different curves relative to the given constraints:
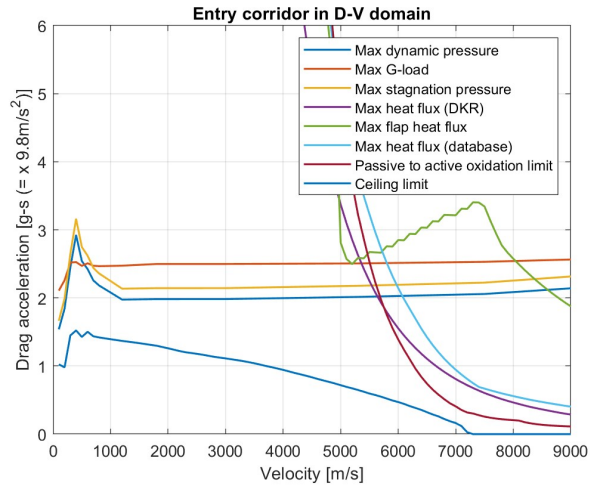
Figure 5.6: Entry corridor with the given constraints

The inferior boundary of the entry corridor is defined by the ceiling limit, the superior boundary is represented by the constraint that has the lower value at a given velocity. The entry corridor can thus be expressed in the following lighter form:
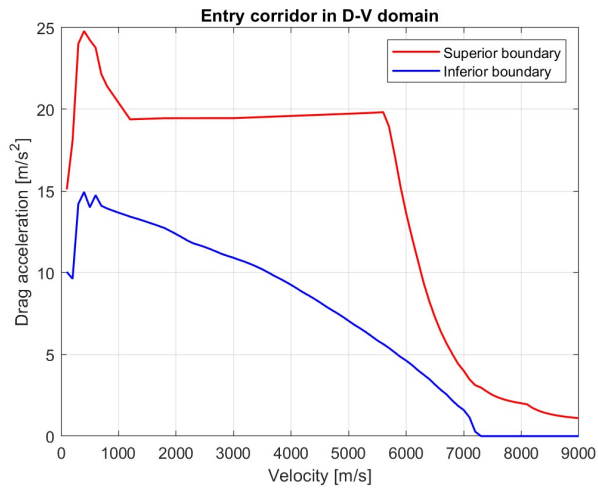
Figure 5.7: Entry corridor boundaries

39

5.4 Ideal reference profile definition

This part of the model analytically calculates 11 curves contained within the entry corridor boundaries called ideal reference profiles. These curves are parameterized with a parameter k that varies from 0 to 1 with a step of 0.1, this is why there are 11 curves. These curves do not represent the actual profiles that will be followed by the control law but they represent the "skeleton" on which the proper reference profile will be built. This will be clarified in section 5.5, for now these ideal profiles are calculated as follows:

The ideal reference profiles are defined by three different functions depending on the velocity of the spacecraft:

$$D(v) = \begin{cases} D_1(v) & \text{if } 0 < v < v\left(Mach_{target}\right) \\ D_2(v) & \text{if } v\left(Mach_{target}\right) < v < 8800 m/s \\ D_3(v) & \text{if } 8800 m/s < v < 9000 m/s \end{cases} \quad (5.5)$$

- $0 < v < v\left(Mach_{target}\right)$
  In this range of velocities the drag profile is constant and the drag value satisfies the target dynamic pressure. D_1 is the same for each of the 11 ideal profiles:
$$D_1(v) = D\left(q_{target}\right) \quad (5.6)$$

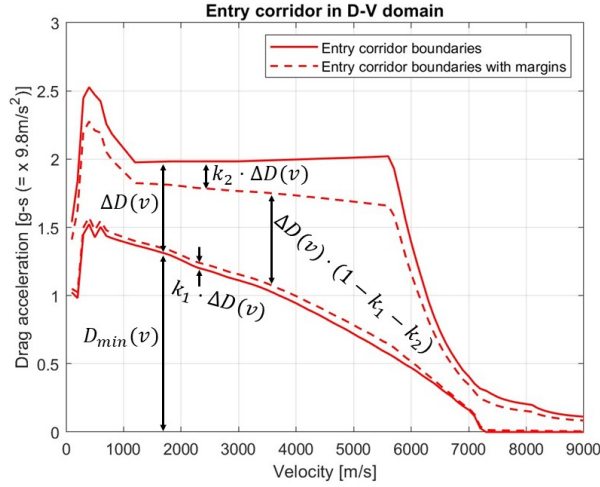- $v\left(Mach_{target}\right) < v < 8800 m/s$
  Here the drag profile is calculated as a spline between different points chosen by the user. The user has to define the following inputs:

  - k_1 and k_2
    $D_{max}(v)$ is the superior boundary of the entry corridor, $D_{min}(v)$ is its inferior boundary and $\Delta D(v) = D_{max}(v) - D_{min}(v)$ is the entry corridor width. k_1 and k_2 represents the margin on these boundaries, meaning that each point of the spline will be contained between $\underline{D_{margin}} = D_{min}(v) + \Delta D(v) \cdot k_1$ and $\overline{D_{margin}} = D_{max}(v) - \Delta D(v) \cdot k_2$:
$$D_2(v) = \underline{D_{margin}} + k \cdot \Delta D(v) \left(1 - k_1 - k_2\right) \quad (5.7)$$

    where $0 \leq k \leq 1$.

Figure 5.8: Entry corridor with margins

– Velocity vector
The user creates a vector of N elements, each element is a velocity value contained between $v\left(Mach_{target}\right)$ and $8800m/s$ in ascending order. These values are the points that will be used for the creation of the spline.

– Upper limit vector
The user can decide if it is desirable to put another upper margin on the drag values. A vector of N elements (same dimension of the velocity vector) is created, the $i-th$ element of this vector is associated with the $i-th$ element of the velocity vector and it must be contained between 0 and 1. If the value is 1 no upper margin (other than the one already defined) is applied, if the value is lower than 1 it means that $k\left(v_i\right)$ is limited to that maximum value.

• $8800m/s < v < 9000m/s$
For this range of velocities the drag is again constant and equal to zero. It is the same for each of the 11 ideal profiles:

$$D_3(v) = 0 \tag{5.8}$$

Finally the 11 ideal reference profiles are obtained with the procedure described above and with $k = 0,0.1,0.2,0.3,...,0.8,0.9,1$ (unless it is saturated by the upper limit vector). The final result is the following:

$$
\begin{cases}
k_1 = 0.05 \\
k_2 = 0.25 \\
V_{vector} = [1500\ 2000\ 3000\ 4000\ 4500\ 5000\ 6000\ 7000] \\
Limit_{vector} = [1\ 1\ 1\ 1\ 1\ 1\ 0.7\ 0.7]
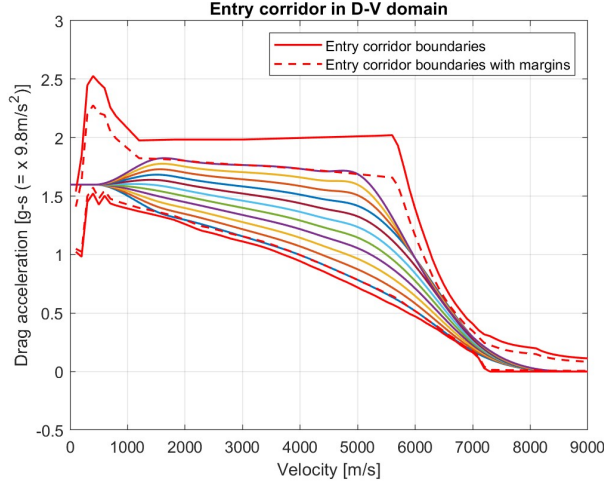\end{cases}
$$

Figure 5.9: Ideal reference profiles

5.5   Reference trajectory optimization model

The optimization model developed in this section finds the gains for the control law described in chapter 4. The goal is to follow with the best accuracy the several ideal reference profiles defined in section 5.4. These gains will be used in section 5.6 to derive the actual reference profile that satisfies every constraint.

This optimization model uses the black-box approach: every constraint is satisfied in the trajectory propagator (the black-box), this makes the problem inherently feasible and the model always converges to a solution, even though this solution might just be a local minimum. This feature makes the model very efficient and fast since its only goal is to minimize a certain cost function.
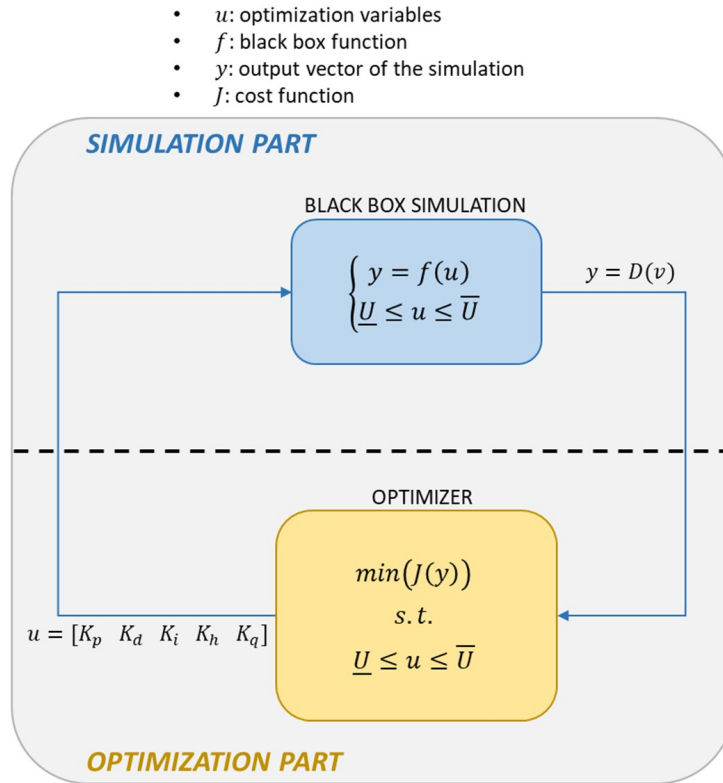
The optimization parameters are the five control gains K_p, K_d, K_i, K_h and K_q. These gains are used in a simplified control law which does not include the bank angle rate limit and the energy management guidance law: the goal is not to reach

the target with high accuracy in terms of position, but to find a profile that stays within the entry corridor boundaries and that satisfies the desired target dynamic pressure when it reaches the target Mach number. This is done by implementing the following cost function that minimizes the square error between the propagated drag-velocity profile and the ideal reference profile:

$$J = \sum_{i=1}^{N} \left(D_{propagated}\left(v_i\right) - D_{ideal}\left(v_i\right) \right)^2 \tag{5.9}$$

N is the number of integration points, it is fixed for a given simulation but it can change between simulations: The trajectory propagator integrates with a fixed time step of 5 seconds and the integration is automatically stopped when the target Mach number is reached.

The trajectory propagator uses the first column of the EIP map as initial conditions and the ideal reference profile followed by the control law is the sixth one (corresponding to $k = 0.5$). Figure 5.10 shows the optimization model block diagram:

- u: optimization variables
- f: black box function
- y: output vector of the simulation
- J: cost function

SIMULATION PART

BLACK BOX SIMULATION

$$\begin{cases} y = f(u) \\ \underline{U} \leq u \leq \overline{U} \end{cases}$$

$y = D(v)$

OPTIMIZER

$$min\left(J(y)\right)$$
$$s.t.$$
$$\underline{U} \leq u \leq \overline{U}$$

$u = [K_p \quad K_d \quad K_i \quad K_h \quad K_q]$
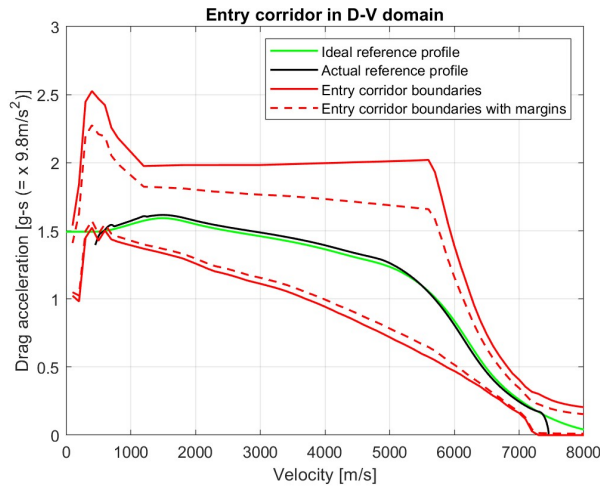
OPTIMIZATION PART

Figure 5.10: Reference trajectory optimization model block diagram

The optimization algorithm is *sqp*, described in section 3.3. The function used to integrate the equations of motion is *ode4*, which is a 4th order fixed step Runge-Kutta method for non stiff problems, the step size is set to 5 seconds.

This optimization model is used inside Matlab Global Optimization Toolbox in order to calculate multiple solutions and hopefully the absolute minimum of the cost function is found. The user has to choose the optimization time and to create a vector of five elements: each element is associated with a certain control gain and represents the maximum value allowed for that specific gain. After the optimization process is complete the user manually chooses the solution that follows in the best way the ideal reference profile and reaches with maximum accuracy the target dynamic pressure:

$$\begin{cases} \text{Optimization time: } 15min \\ [K_{pMAX} \ K_{dMAX} \ K_{iMAX} \ K_{hMAX} \ K_{qMAX}] = [100 \ 2000 \ 1 \ 0.5 \ 10000] \end{cases}$$

Figure 5.11: Reference trajectory optimization model results

$$\begin{cases} \text{Optimal gains: } [67.6 \ 1860.4 \ 0.052 \ 0.292 \ 6326.3 \ ] \\ \text{Final dynamic pressure percentage error: } -6.4\% \end{cases}$$

44

This propagated profile satisfies every constraint but not necessarily the followings:

- Maximum integral heat flux

- Maximum flight time

- Maximum bank angle rate

- No-fly zones

- Ground station visibility

- Target position

Most of these constraints will be satisfied in section 5.6 where the actual reference profile is calculated.
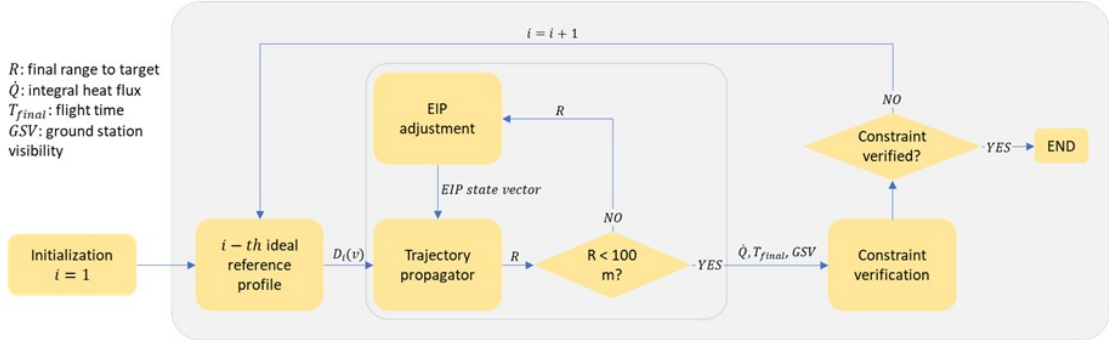
5.6 Actual reference profile calculation

In this section the optimal gains found in section 5.5 are used to propagate the trajectory using each one of the 11 ideal reference profiles calculated in section 5.4, starting from $k = 0$ all the way to $k = 1$. Each time the trajectory is propagated the maximum integral heat flux, maximum flight time and ground station visibility constraints are checked and the first propagated profile that satisfies every constraint becomes the actual reference profile.

The cycle that characterizes this iterative approach is divided in three main parts:

- **selection of the ideal reference profile**
  Here the ideal reference profiles are chosen from the first to the last.

- **Shifting of the EIP point**
  In this part the EIP position is shifted with an iterative process in order to minimize the error on the final position, this is done by interpolating the EIP map table. An accuracy on the target position of less than 100 meters is achievable.

- **Constraints check**
  Here the constraints listed before are verified.

Figure 5.12 shows the block diagram of this iterative process:

Figure 5.12: Actual reference profile calculation block diagram

Figure 5.13 shows the actual drag-velocity and energy-range reference profiles obtained with this process:
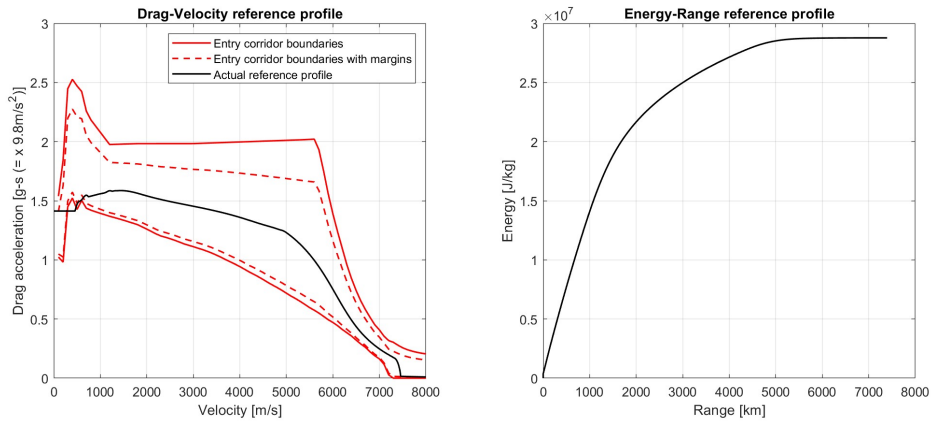
Figure 5.13: Actual reference profile

$$
\begin{cases}
\text{Final position error: } 14m \\
\text{Final dynamic pressure percentage error: } -4.36\% \\
\text{Flight time margin: } 3.5\% \\
\text{Integral heat flux margin: } 71.7\% \\
\text{Ground station visibility margin: } 117\%
\end{cases}
$$

46

This reference profile satisfies every constraint but not necessarily the followings:

- Maximum bank angle rate

- No-fly zones

The no-fly zone will be analyzed in the final parts of this chapter. The maximum bank angle rate is always set to infinity during the trajectory optimization process for a simple reason: if the bank reversal manoeuvres are not instantaneous and instead take a certain amount of time to be finalized, during this time an undesired increased vertical lift component is created. This determines a "bump" on the reference profile each time a bank reversal manoeuvre is commanded and creates noise on the profile itself making it more difficult for the GNC system to follow. By removing the bank angle rate limit on the construction of the reference trajectory, the reference profile obtained is the smoothest possible and the GNC system can follow it more easily.

5.7 Alternative reference trajectory optimization model

The sections 5.7 and 5.8 are necessary only if the optimization model described in sections 5.5 and 5.6 did not find a feasible solution satisfying the constraints. If this is the case a different optimization approach is necessary.

The optimization model described in this section creates a new ideal reference profile by optimizing the drag values of each node used for the spline interpolation. This ideal reference profile is then followed by the control law which utilizes the optimal control gains obtained in section 5.5. The control law is still simplified: it lacks the energy management guidance logic and the bank rate limit.

The optimization strategy still utilizes the black-box approach, most of the constraints are satisfied during the trajectory propagation (black-box part of the model) but some of them are taken into account in the optimization part of the model: integral heat flux and total flight time. This means that the model is not inherently feasible and before minimizing the cost function it needs to find a feasible region for the optimization variables, which is not necessarily guaranteed.

The new ideal reference profile is obtained the following way:

Each spline point P_i is characterized by a X coordinate which is its velocity value v_i, and a Y coordinate which is its drag value D_i:

$$P_i = (v_i, D_i) \tag{5.10}$$

The velocities relative to the N spline points are not chosen by the optimizer model, they are in fact the same values selected by the user in the velocity vector described in section 4.4. The drag values on the other hand are the parameters to be optimized, the model chooses the scale factor k_i for each node:

$$D_i = \underline{D_{margin}} + k_i \cdot \Delta D(v_i)\,(1 - k_1 - k_2) \tag{5.11}$$

With $0 \leq k_i \leq 1$ unless the value is further limited by the upper limit vector described in section 5.4. More details on the terms of the equation 5.11 can be found in the description of equation 5.7. Figure 5.14 shows an example of the ideal reference profiles obtained with this technique, it is important to know that the k_i values in figure 5.14 are not obtained through optimization, they are just random numbers used to demonstrate the concept:
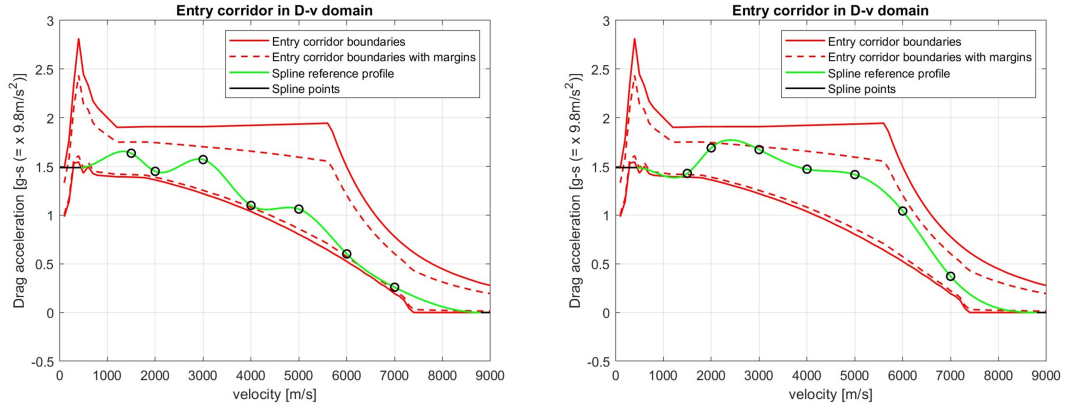
Figure 5.14: Example of ideal reference profile

The cost function and the constraint function are defined the following way:

- **cost function**
  The cost function minimizes the square error between the spline points chosen by the optimizer and the spline points of one of the 11 previous ideal reference profile created in section 5.4. Before the optimization process the user chooses

which one of these 11 ideal profiles has to be used for the calculation of the cost function.

$$J = \sum_{i=1}^{N} \left(D_{ideal_{new}} \left(v_i \right) - D_{ideal_{old}} \left(v_i \right) \right)^2 \tag{5.12}$$

N is the number of spline points.

- **constraint function**
  After the trajectory is propagated, the integral heat flux $\dot{Q}$ and total flight time T are calculated and a constraint function is defined using the following inequality equation:

$$Q = \begin{cases} T - T_{max} < 0 \\ \dot{Q} - \dot{Q}_{max} < 0 \end{cases} \tag{5.13}$$

Figure 5.15 shows the block diagram of this optimization model:
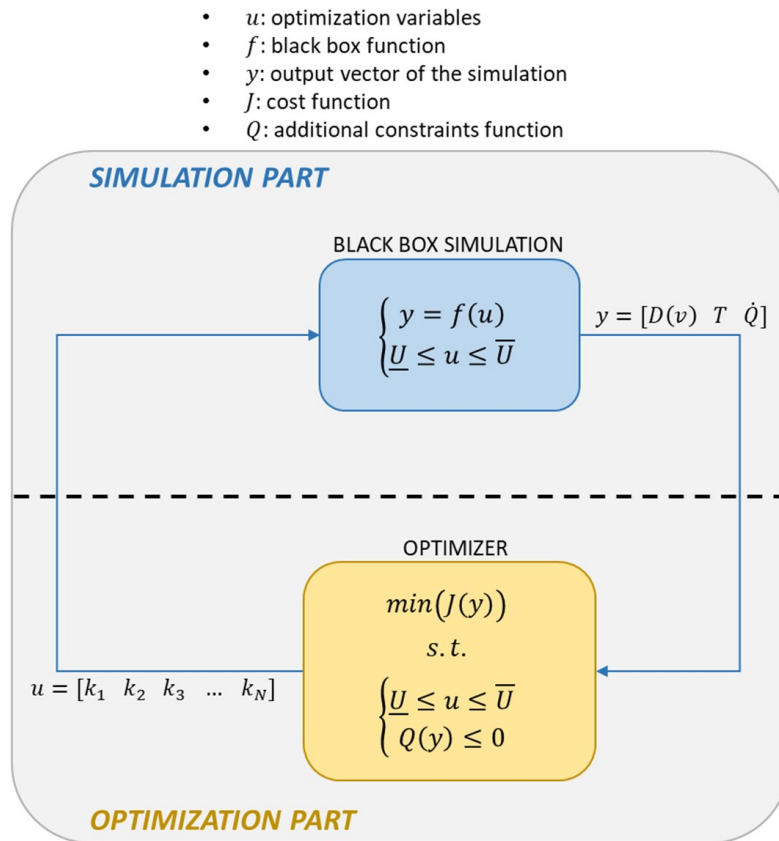
Figure 5.15: Optimizer model 2 block diagram

The optimization algorithm is *sqp*, described in section 3.3. The function used to integrate the equations of motion is *ode4*, which is a 4th order fixed step Runge-Kutta method for non stiff problems, the step size is set to 5 seconds.

This model uses Matlab Global Optimization Toolbox to obtain multiple solutions. Before the optimization process the user chooses the running time. The solutions found by this model satisfy every constraints except the following which might not be satisfied:

- Maximum bank angle rate

- No-fly zones

- Ground station visibility

- Target position

Most of these constraints will be satisfied in the section 5.8 where the actual reference profile is calculated.

5.8   Alternative actual reference profile calculation

In this section the user chooses one of the solutions obtained in section 5.7 to study. Once the profile is chosen, a series of operation similar to what is described in section 5.6 take place:

- **Translation of the EIP point**
  In an iterative process the EIP state vector is interpolated from the EIP conditions map in order to maximize the accuracy on the final position.

- **Constraint check**
  The ground station visibility constraint is checked.

After analyzing every solution obtained in section 5.7, the user chooses the best reference profile considering the following points:

- Ground visibility constraint satisfied

- Smoothness of the profile

- Distance of the profile from the higher boundary of the entry corridor

- Accuracy on the final value of dynamic pressure

At the end of this process the only constraints that are not verified and possibly not satisfied are:

- Maximum bank angle rate

- No-fly zones

The bank angle rate limit will be implemented in section 5.9 where the optimal control gains are calculated.

5.9 Control gains optimization model

In this section the optimal control gains are calculated. The ideal gain values calculated in section 5.5 are optimal when the goal is obtaining the smoothest reference profile but they are not physically feasible. The drawback of being able to follow with extremely high accuracy one of the ideal reference profiles described in section 5.4 is that the resulting bank angle profile has very high frequency and high amplitude oscillations:
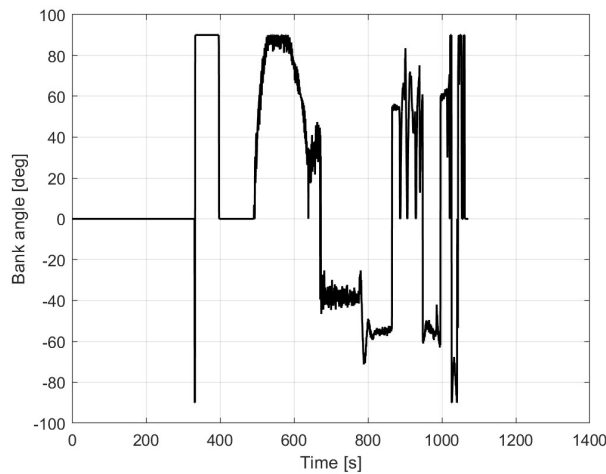
Figure 5.16: Ideal gains bank profile

The solution to this problem is to develop an optimization model which finds control gains that allow the vehicle to precisely follow the actual reference profile and at the same time determine a feasible bank angle profile, which has to be smooth and with limited oscillations.

The model is again developed with a black-box approach: the trajectory propagation part is able to satisfy every constraint and the optimization part has to solve an inherently feasible problem and always converges to a solution. This feature makes the model extremely efficient and fast: in a matter of minutes it is able to find good solutions.

The cost function developed for this goal is a linear combination of two terms:

$$J = \sum_{i=2}^{N} \left((1 - K) \cdot (D\left(v_i\right) - D_{ref}\left(v_i\right))^2 + K \cdot (\sigma\left(v_i\right) - \sigma\left(v_{i-1}\right))^2 \right) \qquad (5.14)$$

N is the number of integration points. The term $(D\left(v_i\right) - D_{ref}\left(v_i\right))^2$ minimizes the error between the propagated drag-velocity profile and the reference drag-velocity, the term $(\sigma\left(v_i\right) - \sigma\left(v_{i-1}\right))^2$ instead minimizes the variations of the bank value throughout the simulation. K is a factor that changes the relative weight of the two terms.

The optimization model uses Matlab Global Optimization Toolbox to obtain multiple solutions. Before the optimization process starts the user has to set the following inputs:

- Duration of the optimization

- A vector containing the maximum values allowed for each gain

- The value of the weight factor K that ranges from 0 (case that minimizes the error between the propagated drag profile and the reference drag profile) to 1 (case that minimizes the bank angle variations)

The control law implemented in the trajectory propagator contains the bank angle rate limit but still lacks the energy management guidance logic. The optimization model block diagram is shown in figure 5.17:

- u: optimization variables
- f: black box function
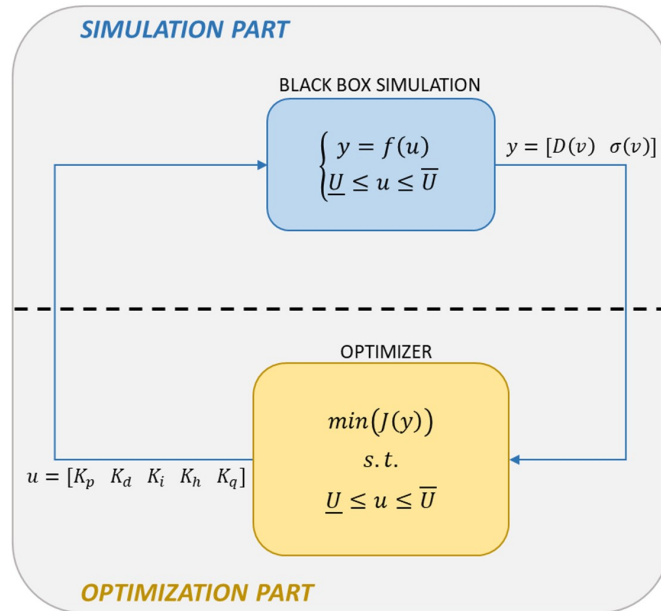- y: output vector of the simulation
- J: cost function

SIMULATION PART

BLACK BOX SIMULATION

$$\begin{cases} y = f(u) \\ \underline{U} \le u \le \overline{U} \end{cases}$$

$y = [D(v) \quad \sigma(v)]$

OPTIMIZER

$$min(J(y))$$
$$s.t.$$
$$\underline{U} \le u \le \overline{U}$$

$u = [K_p \quad K_d \quad K_i \quad K_h \quad K_q]$

OPTIMIZATION PART

Figure 5.17: Optimizer model 3 block diagram

The optimization algorithm is *sqp*, described in section 3.3. The function used to integrate the equations of motion is *ode4*, which is a 4th order fixed step Runge-Kutta method for non stiff problems, the step size is set to 5 seconds. An example of bank angle profile obtained with this technique is shown below:
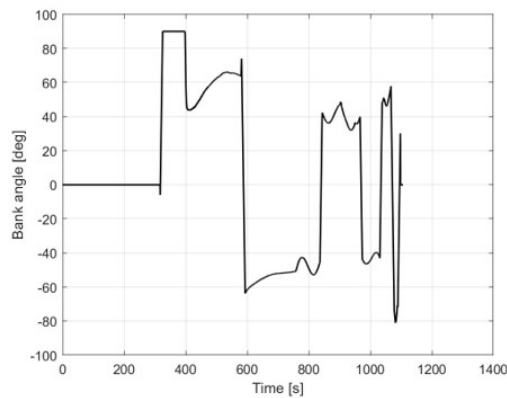
Figure 5.18: Bank angle profile example

53

5.10 Optimal gains choice

In this section the user analyzes the solutions obtained with the third optimization model and chooses the best one. The control law implemented in this part is finally complete and it also contains the energy management guidance logic. The inputs for this section are: the number of the solution that has to be analyzed, the gains of the energy management guidance law K_1 and K_2. In this case 35 solutions were found by the global optimization algorithm, the first three solutions are shown in Figures 5.19, 5.20 and 5.21:
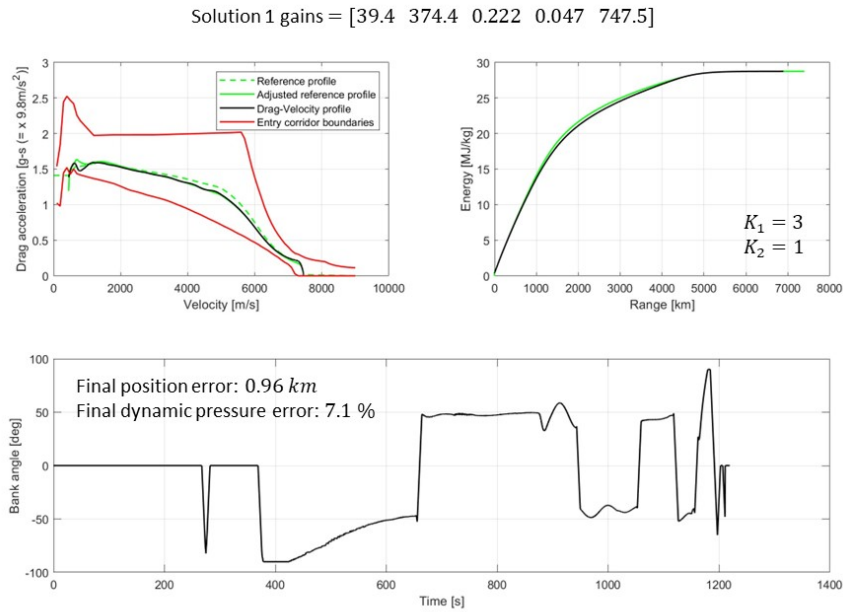
Figure 5.19: Solution 1 profiles

There are mainly four indicators helping the user to choose the best solution. The first indicator is the ability of the vehicle to follow the reference trajectory, visible in the top-left image of figure 5.19. The second indicator is the smoothness of the bank angle profile, visible in the lower image of figure 5.19. The third and fourth indicators are the errors on the final position and dynamic pressure, they must be as small as possible. Solution 1 is acceptable because the reference profile is followed with good precision and the errors on final position and dynamic pressure are minimized. The second and third solutions (Figure 5.20 and 5.21) on the other hand are not acceptable: the second solution has too many oscillations, the third one is completely unable to follow the reference profile adjusted by the energy management guidance logic and it overshoots the entry corridor boundaries in a way that the safety lift term in the control law is not able to counteract:

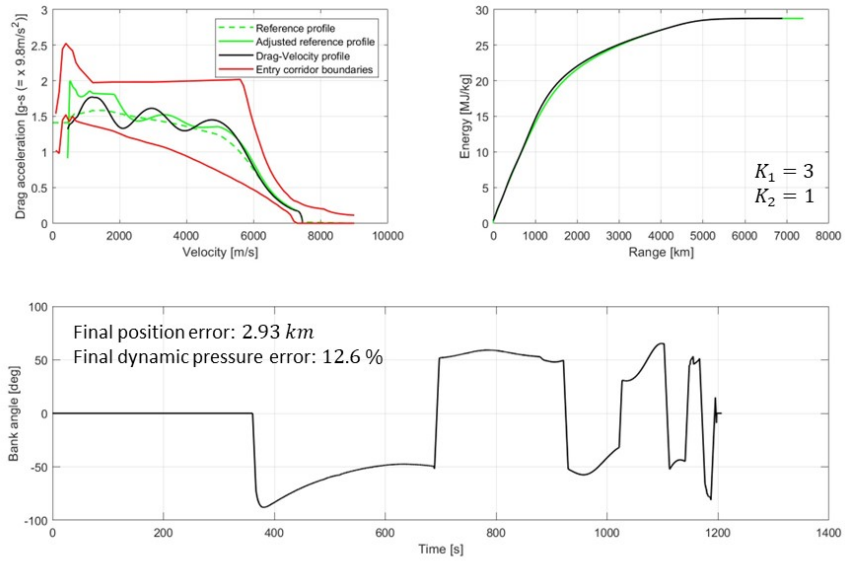Solution 2 gains = [16   135.3   0.025   0.064   309.1]

Figure 5.20: Solution 2 profiles

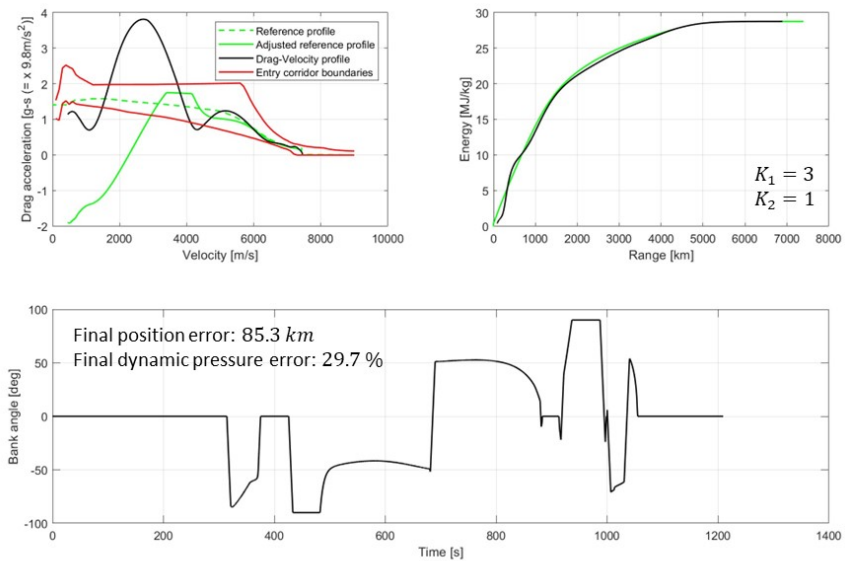Solution 3 gains = [11.2   218.1   0.986   0.358   86.5]

Figure 5.21: Solution 3 profiles

It is important to note that not every time the best solution is the first one, that is why the user must analyze all of them before choosing.

5.11   No-fly zones

The avoidance of the no-fly zones can be implemented in the last part of the optimization process: after many different mission scenarios it has been experimentally proven that it does not change the quality of the solution obtained without considering this aspect. The avoidance strategy includes the definition of waypoints carefully positioned by the user and it is divided in two main parts:

- Calculation of the area where the vehicle can fly.

- Positioning of the waypoints inside this area to avoid the no-fly zone.

These aspects will be discussed in the following subsections.

5.11.1   Region of possible flight

Every vehicle has limited cross-range capabilities, this means that there is a finite region of space where it can safely fly. The calculation of this region is obtained by finding the boundary trajectories: they are the most deviated trajectories flyable by the vehicle where it can still converge to the target.

The boundary trajectories are obtained by using a slightly modified GNC algorithm: the guidance logic for energy management and the control law are kept the same but the guidance logic for bank reversal is modified. Instead of commanding the bank reversal manoeuvre each time the heading error overshoots a certain threshold, there is just one bank reversal throughout the whole trajectory.

The vehicle starts with a given sign of bank angle which does not change for the first part of the trajectory. Then at a specific time T_{switch} the bank reversal manoeuvre takes place and the bank angle sign changes and remains the same for the second part of the trajectory. T_{switch} must be chosen accurately because it is clear that if the bank reversal takes place at time $T = T_{switch} - \Delta T$ the vehicle will undershoot the target, instead if it happens at $T = T_{switch} + \Delta T$ the vehicle will overshoot the target:
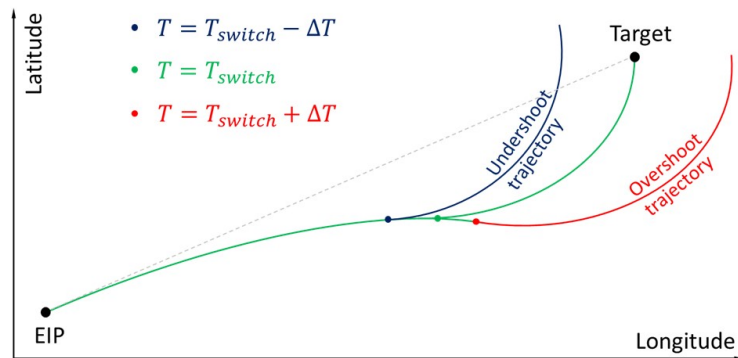
Figure 5.22: Boundary trajectory representation

The time T_{switch} is calculated through an iterative process. In order to define the boundaries of the flyable region two different simulations must be done: the first one starts with a bank angle sign of 1 and then it switches to -1, the second one starts with a bank sign of -1 and then switches to 1. With this process the following result is obtained:
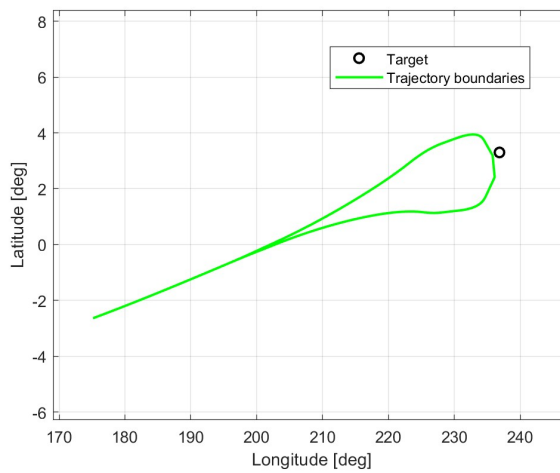
Figure 5.23: Flyable region

The waypoints must be located within this region otherwise the vehicle will not be able to reach them.

5.11.2   Waypoints definition

This section needs several inputs:

- **no-fly value**
  The user sets this value to 1 if there is a no-fly zone, otherwise the value is set to 0.

- **no-fly zone definition**
  The user defines the no-fly zone as a circle characterized by its center co-ordinates and its radius. The first are defined inside a two element vector containing the longitude and the latitude, the second is defined inside a scalar variable.

- **Waypoints definition**
  The waypoints are defined inside a matrix where each line represents a specific waypoint. The first element of each line is the longitude of the waypoint, the second element is its latitude.

- **Initial bank sign**
  The user sets inside a scalar variable the initial sign of the bank angle (1 or -1).

The bank reversal guidance logic considers the first waypoint as its target and the vehicle moves towards it. When the distance between this waypoint and the vehicle becomes smaller than 200 kilometers the bank reversal guidance logic switches to the next waypoint and so on until the target is reached. The user has to tweak the waypoints position in an iterative process in order to avoid the no-fly zone, usually just one waypoint is sufficient for this goal.

Figure 5.24 shows the results of this process together with the ground station visibility:
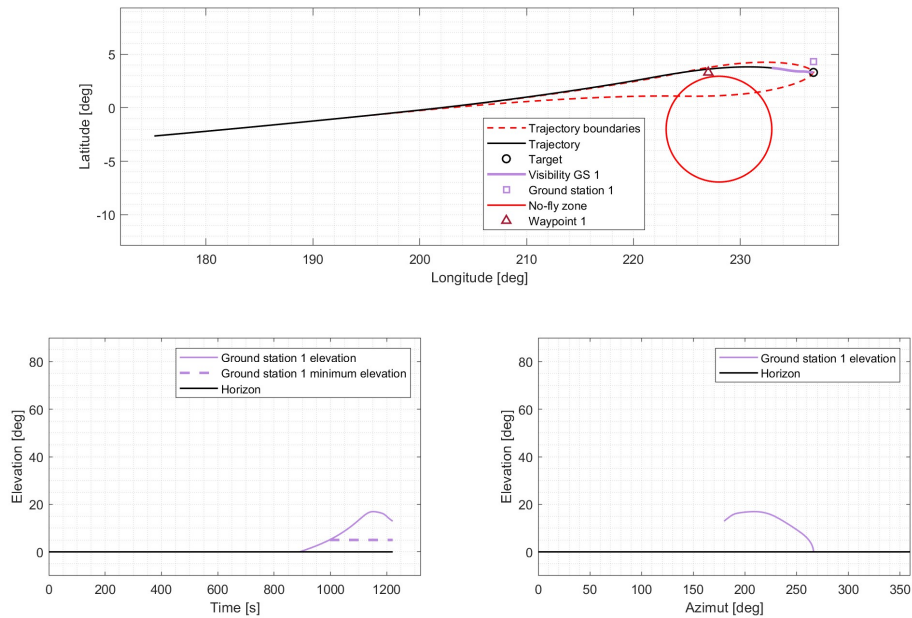

Figure 5.24: Propagated trajectory with waypoint and ground station visibility

5.12   Final trajectory propagator

This is the final part of the process, this trajectory propagator contains the complete GNC algorithms and uses every result from the previous sections. A difference relative to the previous propagators is that here the heat flux is not calculated with the DKR formula but it is interpolated from the IXV aero-thermodynamic database.

This section is mostly used for output visualization as can be seen in figures 5.25, 5.26 and 5.27:
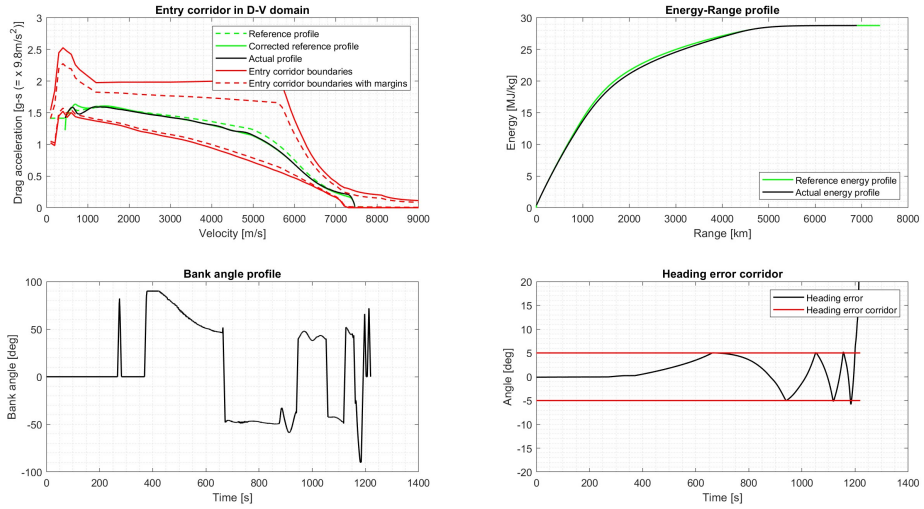
Figure 5.25: Output visualization figure 1
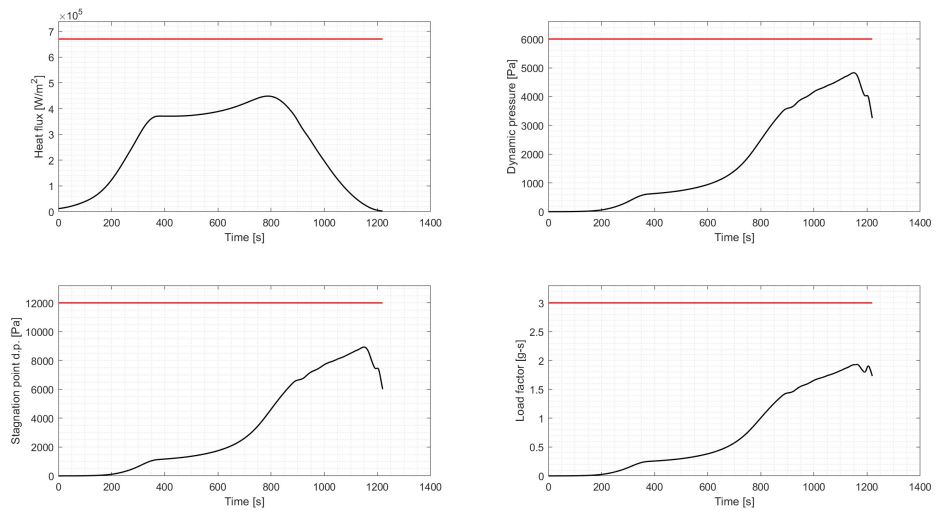
Figure 5.26: Output visualization figure 2
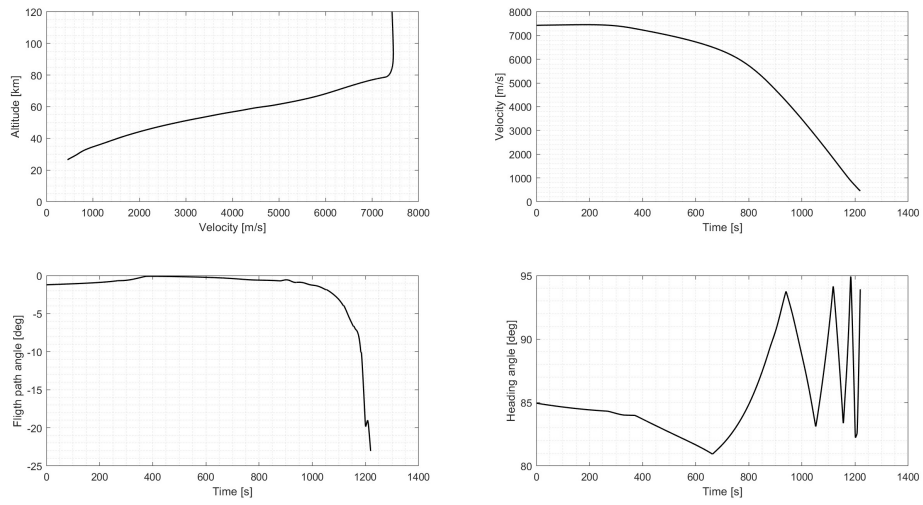
Figure 5.27: Output visualization figure 3

Besides the figures this script also shows the errors between the propagated trajectory and the desired values defined in section 5.1. In this case the errors on the final position and final dynamic pressure are small and acceptable. The other constraints are satisfied since all the margins are positive:

$$\begin{cases} \text{Final position error: } 0.73km \\ \text{Final dynamic pressure percentage error: } -0.14\% \\ \text{Flight time margin: } 2.9\% \\ \text{Integral heat flux margin: } 71.1\% \\ \text{Ground station visibility margin: } 119.5\% \end{cases}$$

Chapter 6

Fixed entry interface point tool

This chapter will discuss the optimization tool that calculates the optimal entry trajectory and the optimal control gains in the case of known initial and final position of the vehicle (EIP and target conditions). The tool has the same structure and it is overall very similar to the one described in chapter 5 with a few differences: instead of having 12 sections it is divided into 9 sections that will be described below.

6.1 Part 1

This part of the chapter describes the first 4 sections of the model which are basically the same as what is shown in sections 5.1, 5.3, 5.4 and 5.5:

- **Model inputs**
  This is the part where every input is declared. It is basically the same as section 5.1 with a main difference: the previous model needed the definition of the orbital parameters, the desired FPA and altitude at the entry interface point in order to calculate the EIP conditions map, necessary for the interpolation of the optimal EIP state vector. In this model instead the EIP conditions are predefined and the user needs to declare only the initial state vector (EIP velocity, radius, longitude, latitude, flight path angle and heading angle).

- **Entry corridor definition**
  The second step is to calculate the entry corridor starting from the defined constraints, this is done the same way described in section 5.3.

- **Ideal reference profile definition**
  This part is exactly the same as what described in section 5.4. The 11 ideal reference profiles are calculated with the same procedure (using a spline with a scale factor k that ranges from 0 to 1) although they will not be used later: in section 6.2 a brand new ideal reference profile will be constructed using an optimal value of the scale factor k, this will be clarified later.

- **Reference trajectory optimization model**
  The goal of this model is to find the optimal control gains able to follow with high precision a generic ideal reference profile in order to start building the actual reference profile. The procedure is the same one described in section 5.5.

6.2   Part 2

This section calculates the actual reference profile that satisfies most of the constraints. The idea is to find the optimal value of k (the scale factor that determines the position of the ideal reference profile inside the entry corridor as seen is section 5.4) that allows the vehicle to end its trajectory exactly at the target position. If $k < k_{optimal}$ then the reference profile is located at higher altitudes and the vehicle overshoots the target; if $k > k_{optimal}$ the reference profile is located at lower altitudes and the vehicle undershoots the target. The problem of finding $k_{optimal}$ can be modeled as the problem of calculating the zero of the following function:
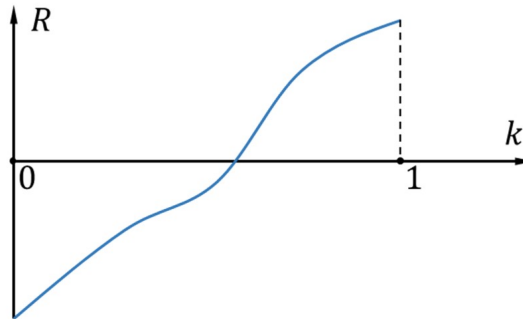
$$R = f(k) \tag{6.1}$$

with $0 < k < 1$
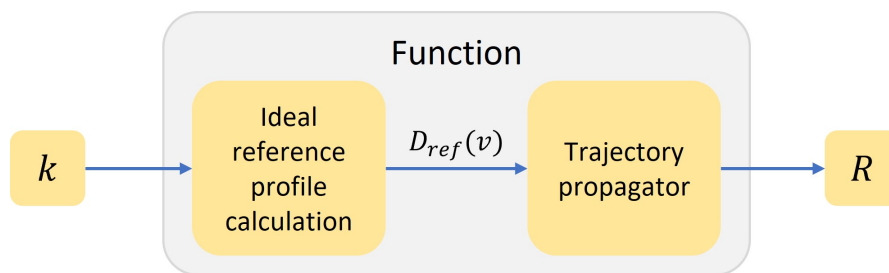
Figure 6.1: Function block diagram

Where R is the final range to target:

Figure 6.2: Function qualitative plot

$k_{optimal}$ that satisfies $R = 0$ is found numerically. The reference profile obtained with this process satisfies every target condition and every constraint plottable in the Drag-Velocity plane.

The biggest problem of this approach is that it finds just one solution, and this solution does not necessarily satisfy the other non-plottable constraints:

- Maximum integral heat flux

- Maximum flight time

- No-fly zones

- Ground station visibility

The no-fly zones are implemented in the final part of the model as seen in section 5.11, and the other three constraints are satisfied in the specific case of the IXV vehicle for its particular trajectory. But a future improvement might be to develop an alternative model that considers these constraints in the optimization process itself.

6.3 Part 3

This part of the chapter describes the last 4 sections of the model which are the same as what is shown in sections 5.9, 5.10, 5.11 and 5.12:

- **Control gains optimization model**
  The optimization model developed in this section calculates the optimal control gains that satisfy the following two conditions: allow the vehicle to follow with precision the reference profile obtained in the previous section, determine a smooth bank angle profile that minimizes the actuators movement. This section is exactly the same as section 5.9.

- **Optimal gains choice**
  Here the user must choose the best solution obtained by the previous optimization model as described in section 5.10.

- **No-fly zones**
  The no-fly zone (if present) is avoided by including one or more waypoints, the process is already described in section 5.11.

- **Final trajectory propagator**
  The complete trajectory propagator that includes the full GNC algorithms is used for output visualization.

Chapter 7

Experimental analysis

This chapter will present the results obtained with the variable entry interface point tool described in chapter 5, many of the comparisons between my results and the ones obtained in IXV mission analysis cannot be shown because of a Non-Disclosure Agreement (NDA) since they are sensible informations.

7.1 Reference framework

The framework of this analysis is the study done in 2014 regarding the IXV vehicle mission analysis. The constraints and boundary conditions used in that document are implemented in the model developed in this thesis to demonstrate the efficacy of the optimization tool and the guidance and navigation algorithms. The informations about the value of constraints, EIP state vector and target state vector are confidential and thus cannot be shown. The comparison will be presented just with relative errors between the different quantities.

7.2 Results and comparison with IXV vehicle

This section shows the results obtained with the fixed EIP re-entry model and compares them to the ones obtained during IXV mission analysis. The values obtained with my model at the end of the trajectory propagation are well within the limits of acceptability and every constraint is satisfied. The percentage difference between the two models is very low, usually less than 5%:

Final state vector		
		Difference
Velocity	[%]	-4,02
Altitude	[%]	-2,27
Longitude	[%]	0,00
Latitude	[%]	0,00
Flight path angle	[%]	-10,46
Heading angle	[%]	-8,04

Figure 7.1: Final state vector

Other quantities		
		Difference
Flight time	[%]	-1,80
Mach number	[%]	0,00
Dynamic pressure	[%]	2,02
Maximum heat flux	[%]	-1,70
Integral heat flux	[%]	0,44
Range to target	[km]	1,19

Figure 7.2: Other quantities

Figure 7.3 compares the reference profile obtained with the tool described in this thesis, to the one obtained during IXV mission analysis. This is the result of the optimization process:
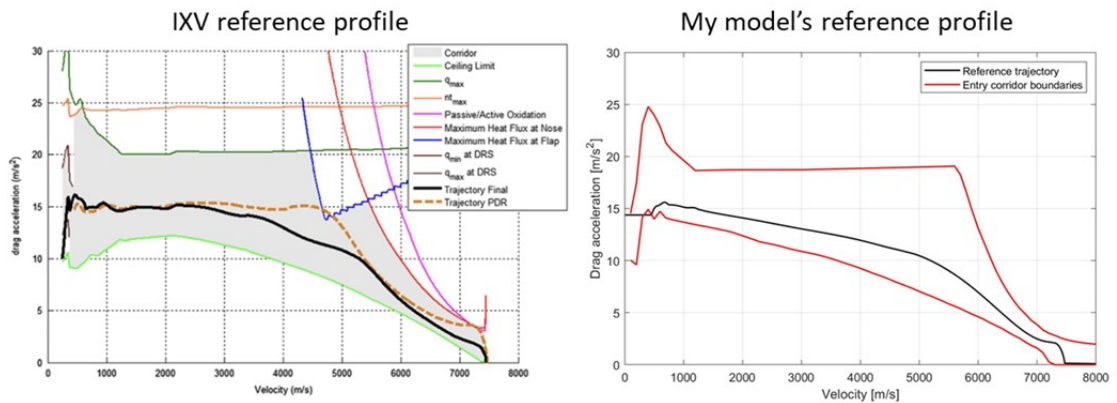
Figure 7.3: Reference profile comparison

The actual Drag-Velocity, Energy-Range and Altitude-Range profiles obtained by propagating the trajectory with the GNC algorithms developed in this thesis are shown below. The optimal control gains found through optimization allow the vehicle to follow with great accuracy the reference profile as can be seen in figures 7.4, 7.5 and 7.6:
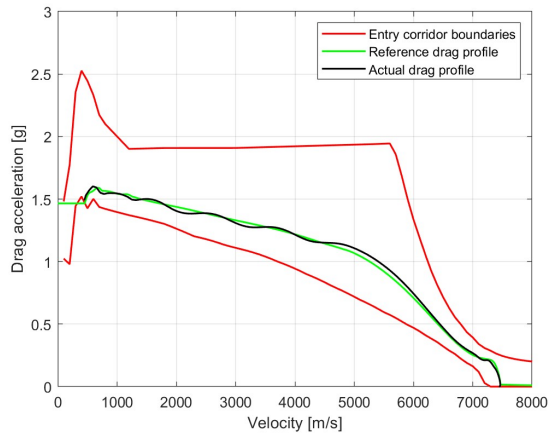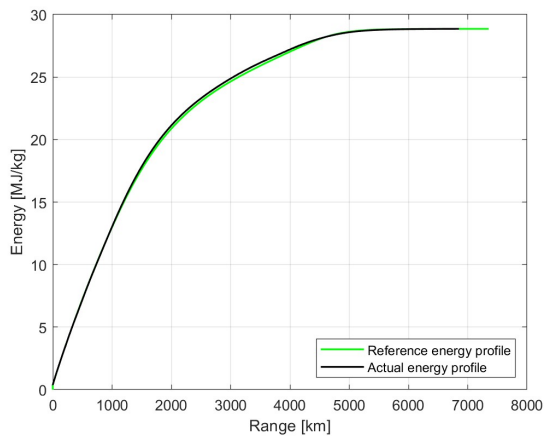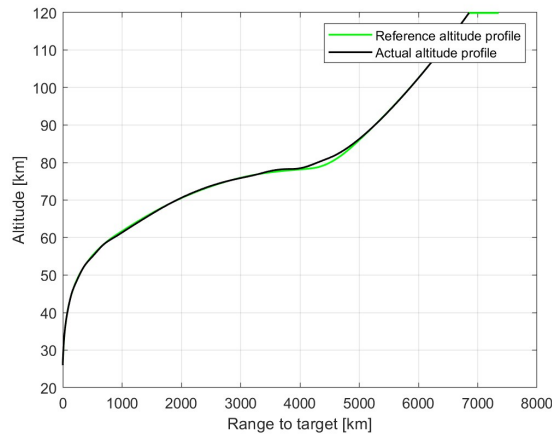

Figure 7.4: Drag-Velocity profile

**Figure 7.5:** Energy-Range profile

Figure 7.6: Altitude-Range profile

The bank angle profile is smooth and two things can be noticed:

- In the first part of the trajectory (first 500 seconds) the control law gets to saturation because it is compensating the fact that the atmosphere is very thin and thus there is not much control authority. When the atmosphere gets denser, the control law scales down its gains and stops saturating.

- Six bank reversal manoeuvres are commanded by the guidance logic and when they happen the bank profile does not change immediately sign: the curve is not vertical but slightly inclined, this is the due to the bank angle rate limitations.
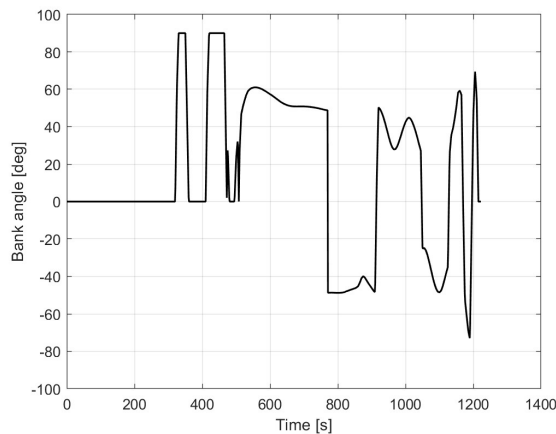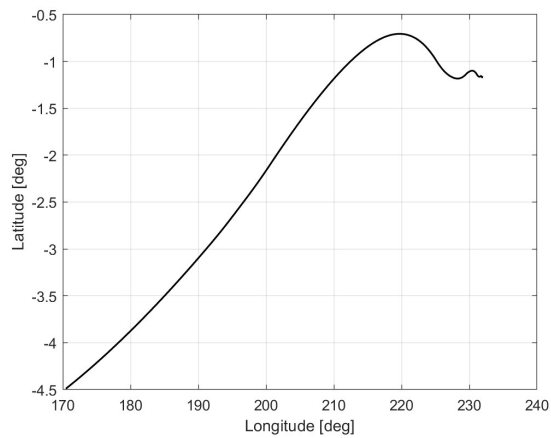

Figure 7.7: Bank angle profile

69

The bank reversal manoeuvres can be clearly noticed in the heading angle profile and also in the projection of the trajectory in the latitude-longitude plane:
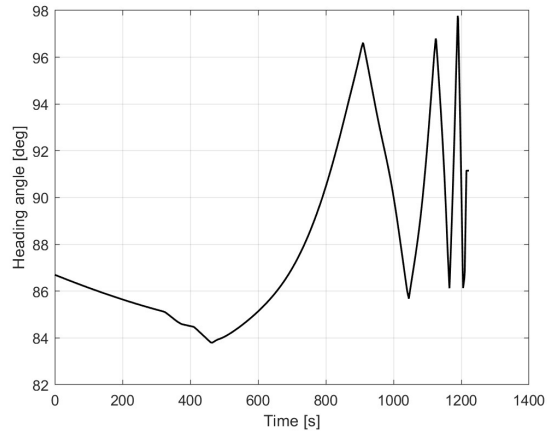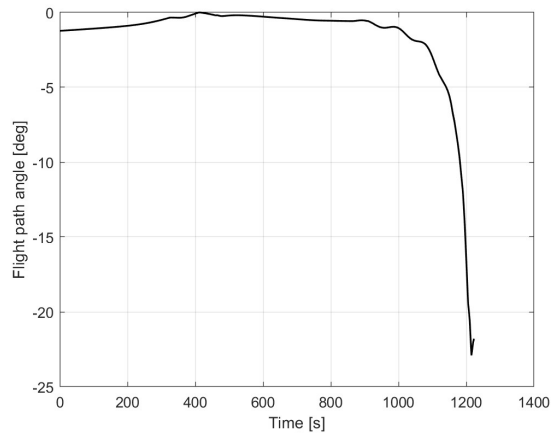

**Figure 7.8:** Heading angle profile

Figure 7.9: Trajectory in the latitude-longitude plane

The flight path angle is almost constant for most of the trajectory and then it decreases significantly in the last parts of the trajectory:
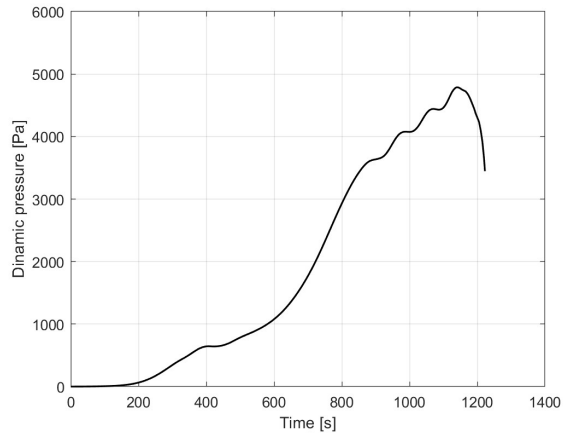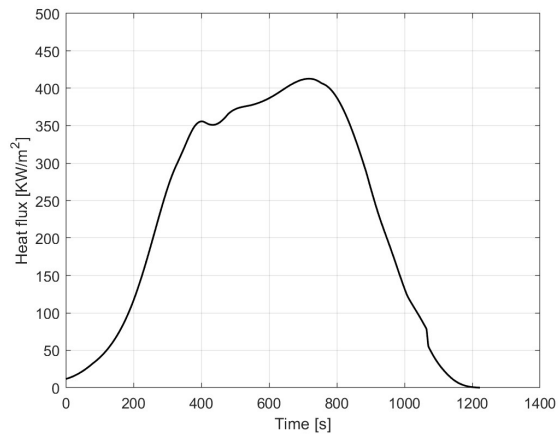

Figure 7.10: Flight path angle profile

The G-load, dynamic pressure, heat flux, total heat flux and passive to active oxidation profiles are well below the maximum allowed values (which cannot be shown because they are proprietary informations). They are presented in figures 7.11 - 7.15:
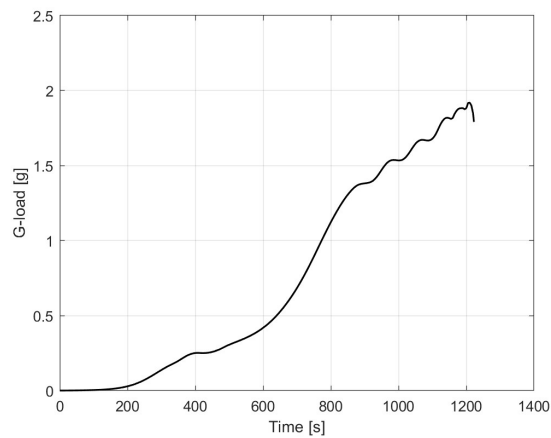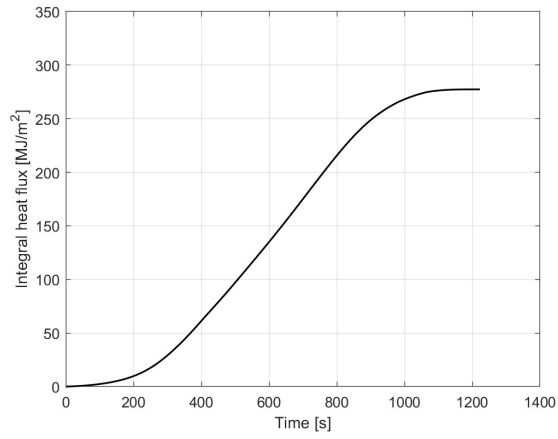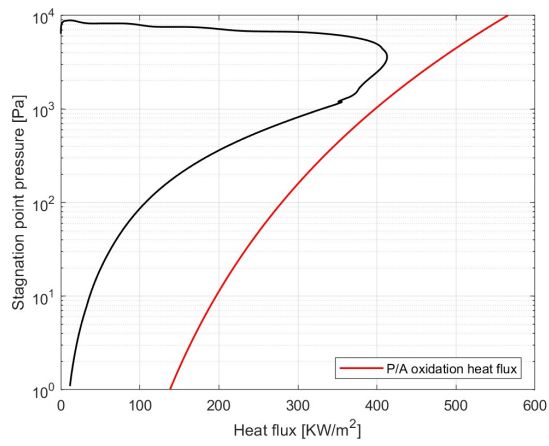

Figure 7.11: G-load profile

71

Figure 7.12: Dynamic pressure profile

Figure 7.13: Heat flux profile

72

Figure 7.14: Total heat flux profile

Figure 7.15: P/A oxidation profile

7.3 Montecarlo analysis

In this section the Montecarlo analysis is shown to prove the robustness of the GNC algorithms developed in this thesis. 1200 cases are analyzed and they all converge to the target and satisfy every constraint. The uncertainties are applied to the following quantities:

- **EIP conditions**
  The EIP conditions uncertainty is applied to the orbital parameters with a normal distribution:

$$\begin{cases} a = a_{nominal} + \Delta a \cdot randn/3 \\ e = e_{nominal} + \Delta e \cdot randn/3 \\ i = i_{nominal} + \Delta i \cdot randn/3 \\ \Omega = \Omega_{nominal} + \Delta\Omega \cdot randn/3 \\ \omega = \omega_{nominal} + \Delta\omega \cdot randn/3 \end{cases} \tag{7.1}$$

  $randn$ is a random number of the normal distribution, it is divided by 3 to contain the 3σ probability within the Δ of the given orbital parameter.

- **Atmospheric conditions**
  Uncertainties are applied to atmospheric density and temperature accordingly to the standard deviations contained in the IXV atmospheric model:

$$\begin{cases} \rho(h) = \rho_{nominal}(h) \cdot (1 + \Delta\rho(h) \cdot randn) \\ T(h) = T_{nominal}(h) \cdot (1 + \Delta T(h) \cdot randn) \end{cases} \tag{7.2}$$

- **Vehicle mass**
  In this case the uncertainty has a constant distribution, not a normal one:

$$m = m_{nominal} + \Delta m \cdot 2 \left(rand - \frac{1}{2} \right) \tag{7.3}$$

  Where $rand$ is a random number between 0 and 1.

- **Trim line**
  The vehicle trim line has the following uncertainty:

$$\alpha(M) = \alpha_{nominal}(M) + \Delta\alpha(M) \cdot randn/3 \tag{7.4}$$

- **Aerodynamic coefficients**
  The aerodynamic coefficients are extracted by IXV aerodynamic database which can optionally implement uncertainties.

- **Mach number at DRS triggering**
  The triggering of the parachute happens at Mach number close to the desired one with a small uncertainty:

$$M_{target} = M_{target_{nominal}} + \Delta M \cdot randn/3 \qquad (7.5)$$

Every uncertainty value is chosen accordingly to what is presented in IXV mission analysis documents. Every propagated trajectory satisfies the different constraints and the target values are within the acceptable margins, the results are shown in figures 7.16 - 7.19:
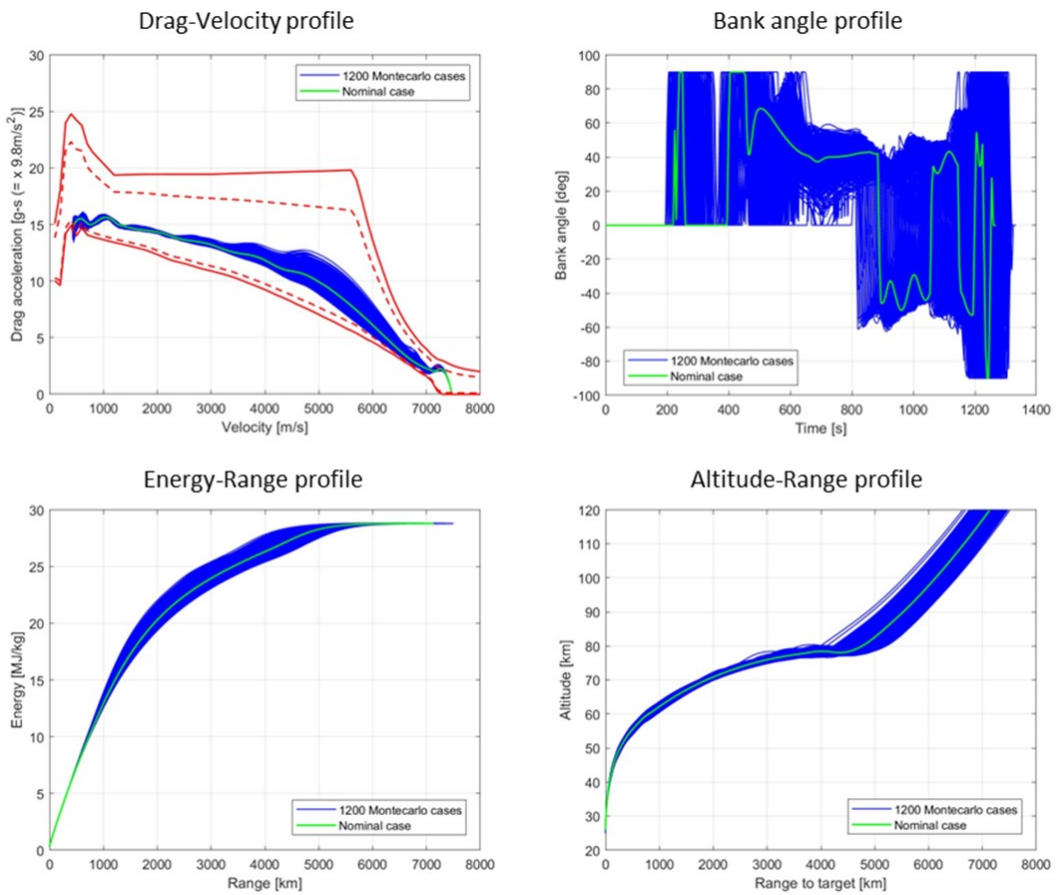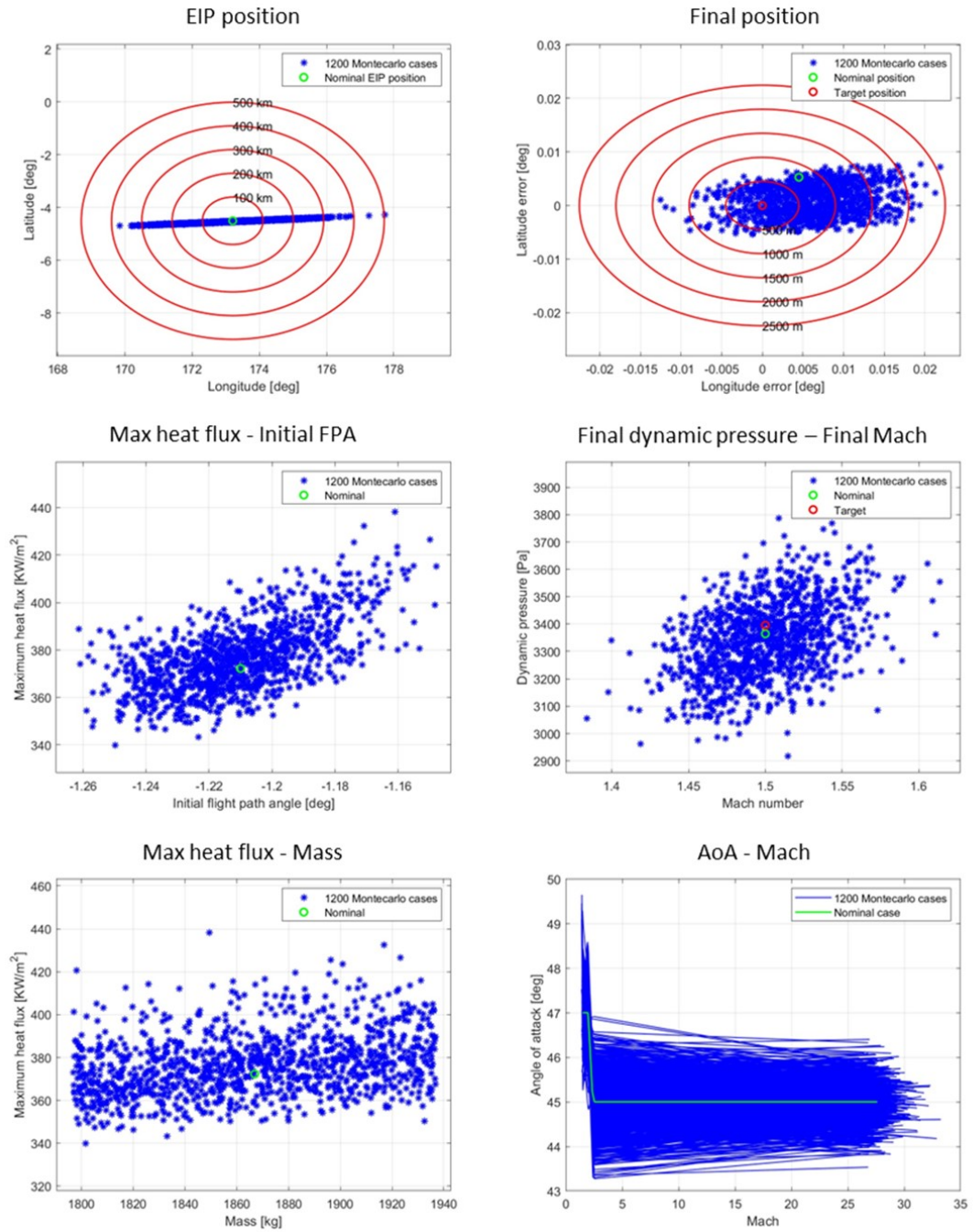

Figure 7.16: Montecarlo results 1
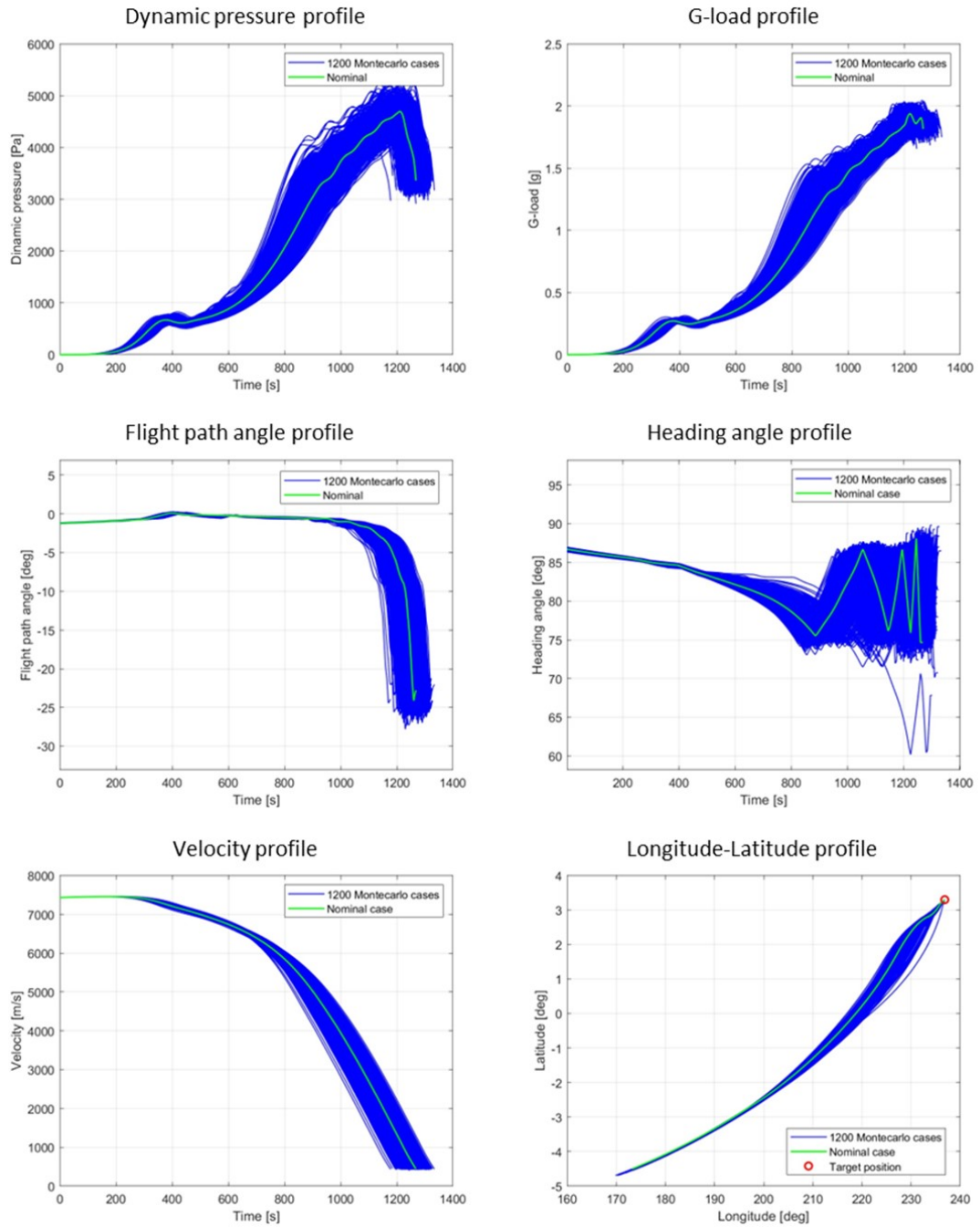
Figure 7.17: Montecarlo results 2

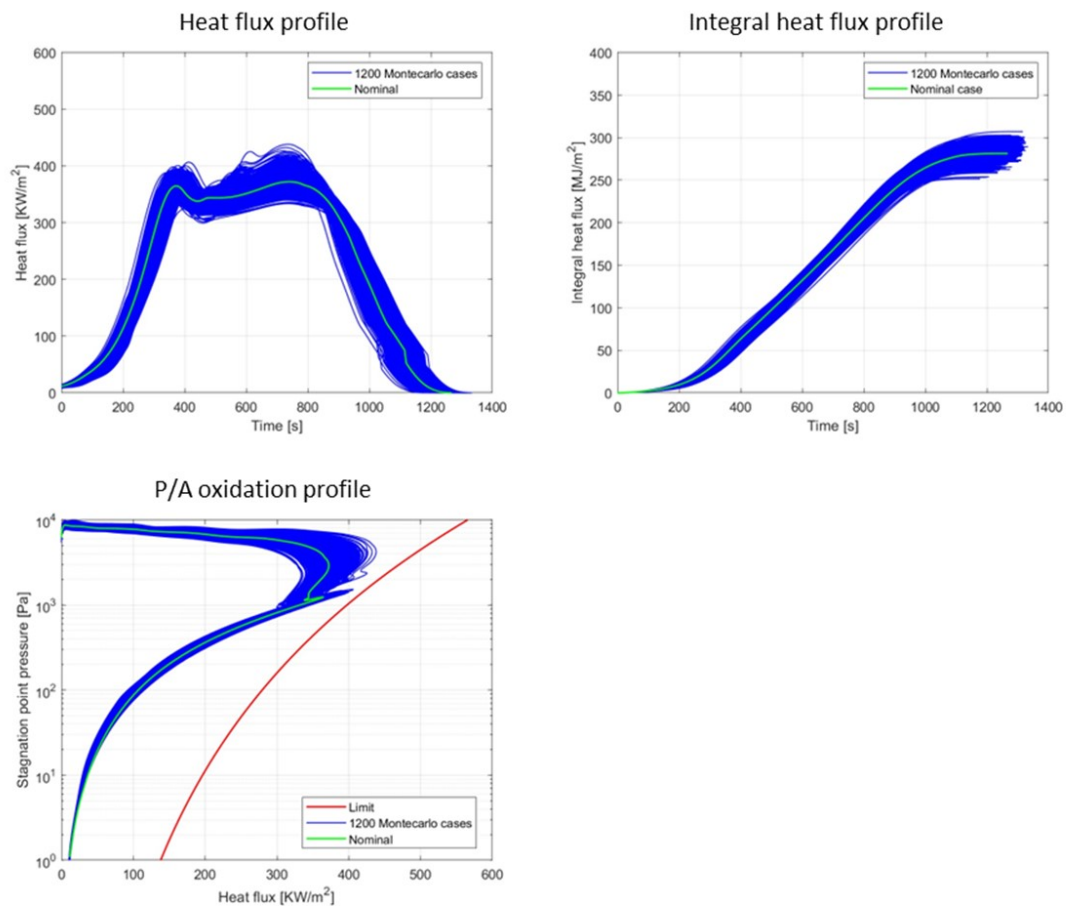**Figure 7.18:** Montecarlo results 3

Figure 7.19: Montecarlo results 4

Chapter 8

Conclusive remarks

The re-entry optimization problem is extremely demanding from a computational point of view. Since the beginning the goal was to develop a fast and efficient optimization tool able to run on average computers in a reasonable amount of time: the model developed in this thesis is the result of this approach.

The trial and error iterative approach exploited in this work resulted in a step by step sequence of relatively simple operations that together allow for the calculation of the optimal reference profile and the optimal gains for the control law. The main advantages of this model are the following:

- **Flexibility**
  By changing values to a set of well defined inputs this model can be applied to many different re-entry scenarios: It can calculate optimal trajectories from every LEO orbit (prograde and retrograde), the target can be located anywhere on the planet and the target conditions can be freely chosen, as well as the constraints. It works with every lifting body vehicle because the optimal gains (that might change depending on the mass, aerodynamic coefficients, maximum bank angle rate, ..., of the spacecraft) are automatically calculated and the guidance and control laws proved to be robust and effective.

- **Adaptability**
  The user can freely change a wide variaty of parameters to obtain maximum performance on a specific re-entry problem.

- **Modularity**
  The step by step approach (12 steps for the variable EIP model described in chapter 5 and 9 steps for the fixed EIP model described in chapter 6) is inherently iterative. After completing the first iteration the solution might be not satisfactory, in this case the user must iterate a second, third, maybe

fourth time. The many steps must be followed in the right order just for the first iteration. From the second iteration the user can change singularly any of the different modules (or steps) without restarting the process from the beginning.

- **Efficient and fast computing**
  The black-box approach used in every optimization model described in this thesis has two main advantages: firstly, the number of optimization variables is very low (never more than 10). Secondly, the minimization of the cost function automatically satisfies every constraint (except one case described in section 5.7) meaning that the problem becomes feasible. It has been demonstrated experimentally that the global optimization tool always finds at least one good local minimum of the cost function for which the feasibility is also implicitly satisfied. These characteristics make the different optimization models described in chapter 5 very fast and the whole tool (from the first to the last step) can be run in under an hour and most likely find a good solution.

- **High precision and accuracy**
  The black-box simulation propagates the trajectory with a fourth order Runge-Kutta method which enables higher accuracy compared to the trapezoid or Simpson methods used in the traditional direct collocation optimization approach.

The comparison of the results with IXV proved the efficacy of the developed tool and the guidance and control algorithms. Some future improvements might be done to enhance the performance and the user experience such as:

- Design a user friendly graphic interface

- Improve the fixed EIP optimization tool which lacks robustness since in some specific cases it might not necessarily satisfy some of the constraints

- Add more constraints such as the maximum flap hinge moment

- Adapt the model to a Martian environment in order to study the feasibility of mars re-entry trajectories.

Bibliography

[1] *Early Reentry Vehicles: Blunt Bodies and Ablatives*. URL: https://www.centennialofflight.net/essay/Evolution_of_Technology/reentry/Tech19.htm (cit. on p. 1).

[2] Regan F.J. and Anandakrishnan S.M. «Dynamics of atmospheric re-entry». In: 1993 (cit. on p. 3).

[3] Hicks K.D. *Introduction to Astrodynamic Reentry*. CreateSpace Independent Publishing Platform, 2014 (cit. on p. 4).

[4] Wingrove R.C. «Guidance and Control in Supercircular Atmosphere Entry». In: *Peaceful Uses of Automation in Outer Space*. Ed. by John A. Aseltine. Springer US, 1966 (cit. on p. 9).

[5] Vinh N.X. «OPTIMAL TRAJECTORIES IN ATMOSPHERIC FLIGHT». In: *Space Mankind's Fourth Environment*. Ed. by NAPOLITANO L.G. Pergamon, 1982 (cit. on p. 12).

[6] Ashish T. *Atmospheric and Space Flight Dynamics: Modeling and Simulation with MATLAB and Simulink*. 1st. Birkhäuser Basel, 2007 (cit. on p. 12).

[7] Haya-Ramos R. Blanco G. Pontijas I. Bonetti D. Freixa J. Parigini C. Bassano E. Carducci R. Sudars M. Denaro A. Angelini R. Mancuso S. «The design and realisation of the IXV Mission Analysis and Flight Mechanics». In: *Acta Astronautica* 124 (2016) (cit. on p. 14).

[8] Nocedal J. and Wright S.J. *Numerical Optimization*. 2e. New York, NY, USA: Springer, 2006 (cit. on p. 15).

[9] Floudas C.A., Akrotirianakis I.G., Caratzoulas S., Meyer C.A., and Kallrath J. «Global optimization in the 21st century: Advances and challenges». In: *Computers Chemical Engineering* 29.6 (2005) (cit. on p. 16).

[10] *Global Optimization Toolbox*. URL: https://it.mathworks.com/help/gads/ (cit. on p. 16).

[11] Becerra V.M. «Practical Direct Collocation Methods for Computational Optimal Control». In: *Modeling and Optimization in Space Engineering.* Ed. by Fasano G. and Pintér J.D. New York, NY: Springer New York, 2013 (cit. on p. 17).

[12] Alarie S., Audet C., Gheribi A.E., Kokkolaras M., and Le Digabel S. «Two decades of blackbox optimization applications». In: *EURO Journal on Computational Optimization* 9 (2021) (cit. on p. 18).

[13] Fletcher R. «The Sequential Quadratic Programming Method». In: ed. by Gianni Di Pillo and Fabio Schoen. Springer Berlin Heidelberg, 2010 (cit. on p. 20).

[14] Burton J. «Descent guidance and mission planning for space shuttle». In: (1985) (cit. on p. 21).